Journal of Medicinal Chemistry

pubs.acs.org/jmc

Article

Prodrugs of a 1-Hydroxy-2-oxopiperidin-3-yl Phosphonate Enolase Inhibitor for the Treatment of *ENO1*-Deleted Cancers

Victoria C. Yan,* Cong-Dat Pham, Elliot S. Ballato, Kristine L. Yang, Kenisha Arthur, Sunada Khadka, Yasaman Barekatain, Prakriti Shrestha, Theresa Tran, Anton H. Poral, Mykia Washington, Sudhir Raghavan, Barbara Czako, Federica Pisaneschi, Yu-Hsi Lin, Nikunj Satani, Naima Hammoudi, Jeffrey J. Ackroyd, Dimitra K. Georgiou, Steven W. Millward, and Florian L. Muller

Cite This: *J. Med. Chem.* 2022, 65, 13813−13832

Read Online

ACCESS | Metrics & More | Article Recommendations | Supporting Information

ABSTRACT: Cancers harboring homozygous deletion of the glycolytic enzyme enolase 1 (*ENO1*) are selectively vulnerable to inhibition of the paralogous isoform, enolase 2 (ENO2). A previous work described the sustained tumor regression activities of a substrate-competitive phosphonate inhibitor of ENO2, 1-hydroxy-2-oxopiperidin-3-yl phosphonate (HEX) (**5**), and its bis-pivaloyoxymethyl prodrug, POMHEX (**6**), in an *ENO1*-deleted intracranial orthotopic xenograft model of glioblastoma [*Nature Metabolism* **2020,** *2,* 1423−1426]. Due to poor pharmacokinetics of bis-ester prodrugs, this study was undertaken to identify potential non-esterase prodrugs for further development. Whereas phosphonoamidate esters were efficiently bioactivated in *ENO1*-deleted glioma cells, McGuigan prodrugs were not. Other strategies, including cycloSal and lipid prodrugs of **5**, exhibited low micromolar IC_{50} values in *ENO1*-deleted glioma cells and improved stability in human serum over **6**. The activity of select prodrugs was also probed using the NCI-60 cell line screen, supporting its use to examine the relationship between prodrugs and cell line-dependent bioactivation.

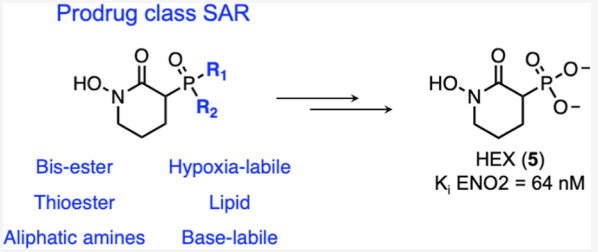

INTRODUCTION

Glycolysis inhibition is an aspirational therapeutic target in cancer therapy, as elevated glycolytic flux facilitates cellular growth and proliferation.[1−3] However, as glycolysis is an essential metabolic process for all cells, developing therapeutics that possess a sufficiently wide therapeutic window between cancer and normal cells has remained a persistent challenge.[4] We previously identified a subset of 1p36 homozygous deleted cancers harboring passenger deletions of the gene encoding the glycolytic enzyme enolase 1 (*ENO1*).[5,6] Such cancers, which include poorly prognosed subtypes, such as glioblastoma (GBM), hepatocellular carcinoma, cholangiocarcinoma, and large-cell neuroendocrine tumors, are exceptionally sensitive to pharmacological inhibition of the paralogous minor isoform, ENO2 (Figure 1a,b).[7,8] Because homozygous deletion of *ENO1* is a cancer-specific event, inhibition of ENO2 results in selective killing of cancerous but not normal cells.

Enolase catalyzes the dehydration of 2-phosphoglycerate (2-PG) to phosphoenolpyruvate (PEP) in the penultimate step of glycolysis (Figure 1a). In an effort to identify suitable inhibitors of enolase, we first turned to the literature and found phosphoacetohydroxamate (PhAH, **1**; PDB: 4ZA0) to be the most potent, substrate-competitive, pan-enolase inhibitor described at the time.[9] Using PhAH as a starting point, we conducted molecular docking studies to identify derivatives with improved specificity for human ENO2.[8] Human *ENO1* and ENO2 share 84% sequence identity—bearing even higher resemblance in the active site.[10,11] Maximizing inhibitor specificity for ENO2 was an important design goal to avoid inhibition of erythrocytic *ENO1*—the sole isoform present in erythrocytes—which can result in anemia.[12,13] With these constraints, we identified a cyclic derivative of PhAH, deoxySF2312 (**2**), which bore close resemblance to the natural product antibiotic, SF2312 (**3**; PDB: 4ZCW).[8] We clarified the stereochemical requirements for active site binding by SF2312 by synthesizing a Cα-methyl derivative of SF2312 (mSF2312, **4**; PDB: 5EU9), which showed that ENO2 binding was specific to the 3*S*, 5*S* enantiomer.[14] Further structure−activity relationship (SAR) studies aimed at improving ENO2 specificity led to the identification of 1-hydroxy-2-oxopiperidin-3-yl phosphonate (HEX, **5**; Figure 1, PDB: 5IDZ).[12] Of these four candidates (Figure 1c), we focused on the development of **5** due to its clear preference for ENO2 at lower concentrations and lower

Received: June 30, 2022
Published: October 17, 2022

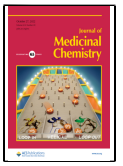

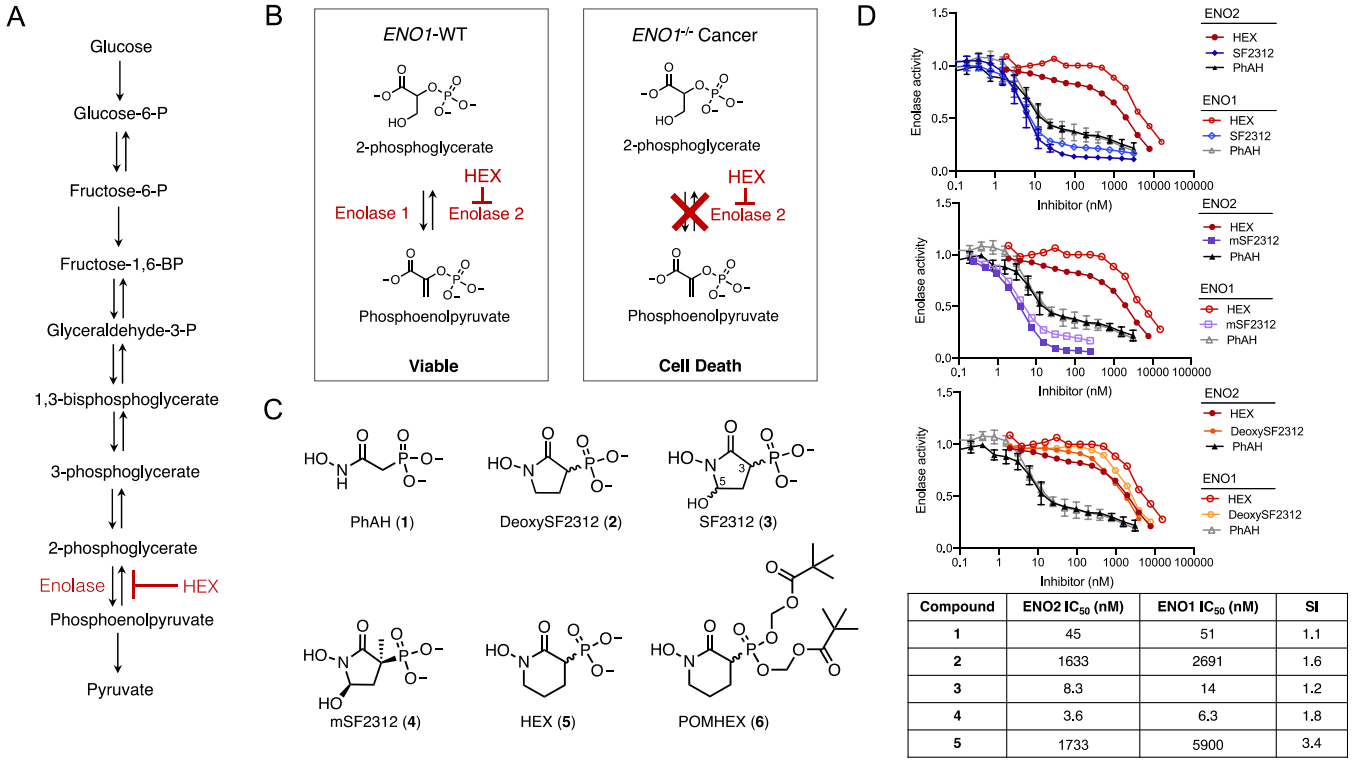

Compound	ENO2 IC_{50} (nM)	ENO1 IC_{50} (nM)	SI
1	45	51	1.1
2	1633	2691	1.6
3	8.3	14	1.2
4	3.6	6.3	1.8
5	1733	5900	3.4

Figure 1. HEX is a phosphonate inhibitor of enolase with four-fold preference for ENO2. (A) Glycolysis pathway. Enolase catalyzes the penultimate step of glycolysis. (B) Collateral lethality schematic in the context of *ENO1*/2. Cancers harboring passenger deletion of *ENO1* at the 1p36 chromosomal locus are uniquely susceptible to inhibition of ENO2. In contrast, inhibition of ENO2 in normal or *ENO1*-WT cells remains viable. (C) Structures of active site enolase inhibitors. POMHEX (**6**) is a cell-permeable prodrug of HEX (**5**). (D) Inhibitory kinetics of enolase inhibitors at 5 mM 2-PG. Pan-enolase inhibitor PhAH (black, gray) and ENO2-preferred inhibitor HEX (red) are compared to either SF2312 (blue, top graph), mSF2312 (purple, middle graph), or deoxySF2312 (orange, bottom graph). Data presented are the mean ± SD of $N \geq 5$.

molecular complexity, which eases the synthesis of prodrug derivatives (Figure 1d).

As a phosphonate inhibitor, **5** is a dianion at physiological pH and is poorly cell- and tissue-permeable. We thus sought to generate lipophilic prodrug derivatives of **5**, as had been done for many clinically impactful phosph(on)ate-containing nucleotide analogues in the antiviral field.[15−17] Our initial synthesis efforts were geared toward rapidly testing the in vivo viability of collateral lethality as a therapeutic paradigm in the context of *ENO1*$^{-/-}$ GBM.[6] Accordingly, we first synthesized the bis-pivaloyloxymethyl (POM) prodrug of **5** (POMHEX, **6**, Figure 1c), the simplest ester prodrug with an extensive precedent for enabling efficient cell permeability and rapid intracellular release of phosph(on)ate drugs.[15,16,18−20] Indeed, owing to improved cell permeability, **6** was approximately 40-fold more potent than the parent **5** against *ENO1*$^{-/-}$ glioma cell lines D423 and Gli56 in vitro (IC_{50} = 0.03−0.09 vs 1.3 μM for **6** and **5**, respectively).[12,21] Against the *ENO1* isogenic rescue cell line, D423 *ENO1*, and the *ENO1*-wild-type (WT) cell line LN319, neither **6** nor **5** exhibited dose-dependent toxicity, which concurs with the hypothesized mechanism of genomically defined, selective killing. Consistent with pharmacodynamic engagement at the enolase reaction, treatment with either **6** or **5** produced upstream accumulations of glycolysis metabolites and downstream depletions of anaplerotic metabolites, and the extent of this metabolic effect correlated with the *ENO1*-deletion status of the cell line tested.[12,21] Against *ENO1*$^{-/-}$ intracranial orthotopic tumors in mice, treatment with either **6** (10 mg/kg IV and IP) or **5** (150 mg/kg IV and 100 mg/kg IP) resulted in profound tumor regression and long-term survival even after drug discontinuation.[12] These data provided solid in vivo proof-of-principle on the viability of collateral lethality as a therapeutic paradigm but also revealed areas for improvement related to promoiety identity on **5**. Being an esterase-labile prodrug, **6** was susceptible to rapid hydrolysis by plasma esterases (Figure S3), which resulted in significant inhibition of enolase in visceral organs such as the heart.[12] While no drug-related adverse events were observed during the 50 day in vivo evaluation of **6**, this finding was a concern and provided strong impetus for us to conduct prodrug optimization studies on **5**.

We were interested in developing second-generation prodrugs of **5** with the primary goal of identifying non-esterase-labile prodrugs that would also lead to the rapid intracellular release of **5** in target cancer cells. Pharmacologically, our pursuit of the ideal prodrug of **5** is also a continuation of our aim to improve its cell, tissue, and—potentially—the brain permeability. Finally, a cancer-specific prodrug of **5** coupled with a genomically rationalized target would further widen the therapeutic window between cancer and normal cells: this could open the possibility of targeting *ENO1*-heterozygous-deleted cancers, which comprise a larger patient population. During our screening, we also identified several novel promoieties with distinct mechanisms of bioactivation from reported phosph(on)ate prodrug strategies (e.g., Farquhar, McGuigan/ProTide, and HepDirect), which may be of interest to those in the phosph(on)ate prodrug field.[18,22−24] Here, we describe the in vitro activity of some novel prodrugs of **5** for the treatment of glycolysis-deficient cancers.

https://doi.org/10.1021/acs.jmedchem.2c01039
J. Med. Chem. 2022, 65, 13813−13832

Scheme 1. Phosphonate Prodrugs of 5[a]

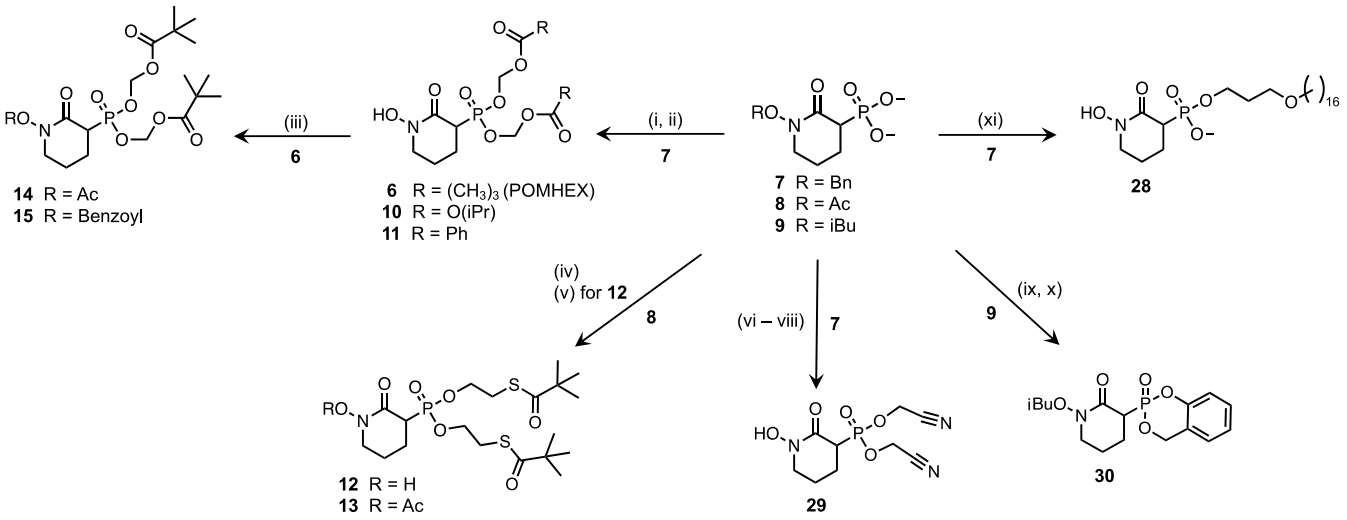

[a]Reagents and conditions: (i) Et_3N, chloromethyl pivalate, chloromethyl isopropyl carbonate, or benzyl chloromethyl ether, MeCN, 50 °C, 24 h; (ii) H_2, Pd/C, THF/MeOH, 1 h. Yields over two steps: 60% (**6**), 69% (**10**), and 64% (**11**); (iii) Et_3N, acetic anhydride (70% for **14**), benzoic anhydride (63% for **15**), MeCN; (iv) *S*-(2-hydroxyethyl) 2,2-dimethylpropanethioate, Mitsunobu conditions (see the Experimental Section), CH_2Cl_2 (10%); (v) Cs_2CO_3, MeCN, 10 min (70%); (vi) $SOCl_2$, DMF, neat (97%); (vii) 2-cyanoethanol, CH_2Cl_2 (88%); (viii) H_2, Pd/C, THF/MeOH, 30 min; (ix) $SOCl_2$, DMF, neat (97%); (x) DBU, 2-(hydroxymethyl)phenol, CH_2Cl_2, (39–65%); (x) 3-(hexadecyloxy)propan-1-ol, *N*,*N*′-dicyclohexylcarbodiimide, py (48%); (xi) H_2, Pd/C, THF/MeOH, 3 h (76%).

Table 1. SAR of Prodrugs of 5[a]

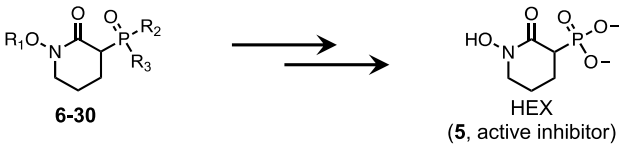

cpd.	R_1	R_2	R_3	IC_{50} (nM) D423 (*ENO1*$^{-/-}$)	IC_{50} (nM) D423 (*ENO1*-tg)[b]	IC_{50} (nM) LN319 (*ENO1*$^{+/+}$)	log *D*[c]
5	H	−OH	−OH	1300	>300,000	>300,000	−4.16
6	H	POM	POM	43	1184	4900	2.80
10	H	POC	POC	16	ND	4276	1.99
11	H	methyl benzoate	methyl benzoate	46	3136	12,769	3.51
12	H	SATE	SATE	124	10,221	2043	3.12
13	Ac	SATE	SATE	19	10,072	1907	3.58
14	Ac	POM	POM	16	ND	679	3.18
15	Bz	POM	POM	39	ND	1728	5.31
16	H	L-alanine isopropyl ester	L-alanine isopropyl ester	2874	>100,000	>100,000	−0.11
17[d]	H	phenol	L-alaninate isopropyl ester	18	671	5091	1.21
18[d]	H	naphthol	L-alaninate isopropyl ester	36	2691	9042	2.21
22	Ac	SATE	benzylamine	19	10,072	1907	2.71
23	Ac	SATE	2-picolylamine	71	1279	15,373	1.64
24 (21% O_2)	H	(5-nitrofuran-2 yl)methanol	benzylamine	299	38,699	33,113	1.48
24 (1% O_2)	H	(5-nitrofuran-2 yl)methanol	benzylamine	171	5746	7840	
25	H	2-cyanoethanol	benzylamine	6676	>70,000	775	−0.10
26	H	4-fluorophenol	benzylamine	>100,000	>100,000	>100,000	2.19
27	H	methyl[1,4′-bipiperidine]-1′-carboxylate	benzylamine	36,860	ND	>100,000	−0.52
28	H	3-(hexadecyloxy)propanol	−OH	207	291	681	2.72
29	H	2-cyanoethanol	2-cyanoethanol	>100,000	ND	>100,000	−1.68
30	*i*Bu	2-(hydroxymethyl)phenol		625	22,600	37,024	2.27

[a]Data are presented as the mean of $N \geq 2$. Full structures are available in the Supporting Information. [b]D423 *ENO1* is an isogenically rescued control cell line in which *ENO1* has been ectopically re-expressed in D423 cells. [c]Values calculated from Chemicalize. [d]10 day incubation.

https://doi.org/10.1021/acs.jmedchem.2c01039
J. Med. Chem. 2022, 65, 13813−13832

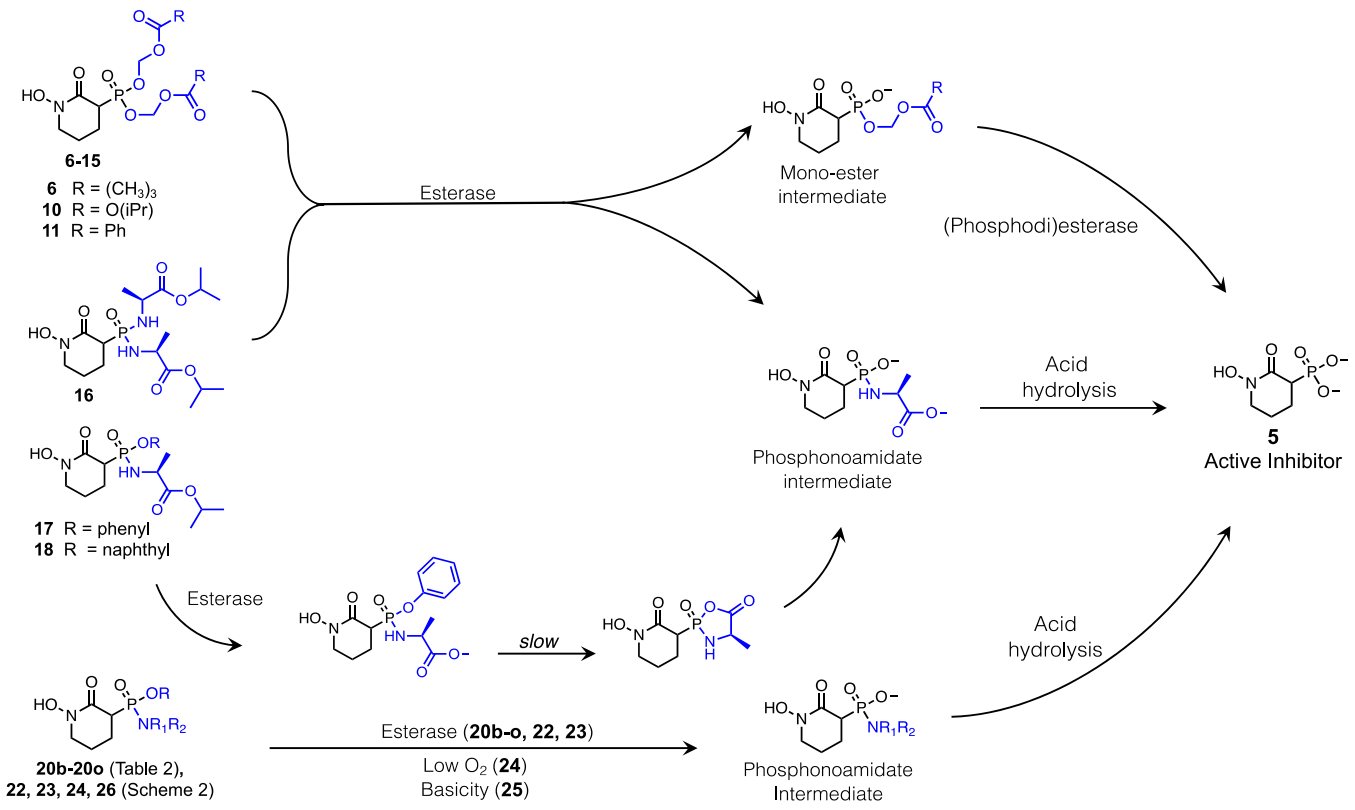

Figure 2. Proposed intracellular bioactivation of prodrugs of **5**. For esterase-labile prodrugs **6**−**15**: two-step intracellular bioactivation. Initial hydrolysis of the first ester group occurs via carboxylesterases. For bis-POC prodrug **11**, hydrolysis of the second ester group can occur via (carboxyl)esterase hydrolysis of the terminal isopropyl ester. In contrast, bis-esters **6**, **12**−**15** undergo second hydrolysis via phosphodiesterases. For bis-amidate prodrug **16**: esterase hydrolysis yields a phosphonoamidate intermediate, which is susceptible to acid hydrolysis toward **5**. For McGuigan prodrugs **17** and **18**, initial esterase hydrolysis of the terminal isopropyl ester is followed by an intramolecular cyclization step that is hypothesized to be inefficient due to the higher-order substitution of Cα on **5**. For phosphoamidate prodrugs: **20b**−**20o**, **22**, and **23** are initially hydrolyzed by esterases, **24** is hydrolyzed under basic conditions, and **26** is hydrolyzed under hypoxic conditions. All phosphoamidate prodrugs converge on a common phosphonoamidate intermediate, which is then hydrolyzed under acidic conditions toward **5**.

RESULTS AND DISCUSSION

The syntheses of **5** and **6** were described previously.[12] To ensure the activity of novel prodrugs synthesized was the result of prodrug bioactivation, followed by on-target inhibition of enolase; all prodrugs were tested for 6 days in an in vitro system consisting of three glioma cell lines: D423 (*ENO1*$^{-/-}$), D423 *ENO1* (*ENO1*-isogenic rescue), and LN319 (*ENO1*$^{+/+}$), unless otherwise stated. If prodrugs exhibited selective dose-dependent toxicity exclusive to the D423 cell line, then, we determined that the promoieties were successfully cleaved, leading to inhibitory activity by **5**. Comparing the calculated IC_{50} values in D423 cells informed the efficiency of prodrug bioactivation. While our end goal was to identify a non-esterase-labile prodrug of **5**, we began our prodrug expedition by synthesizing several ester prodrugs with an established precedent. Because most SAR studies with phosph(on)ate prodrugs have been conducted on nucleotide analogues,[25] we sought to validate the efficiency of these delivery strategies on **5**, a structurally dissimilar, non-nucleotide phosphonate.

Evaluating the Efficacy of Canonical Bis-Ester Prodrugs. We first evaluated a series of bis-ester prodrug strategies, including isopropyloxymethyl carbonate (POC) and *S*-acyl-2-thioethyl (SATE; Scheme 1, Table 1, compounds **6**−**13**). Bioactivation of bis-ester prodrugs proceeds through a common pathway first involving carboxylesterases and then (phosphodi)esterases (Figure 2), which are ubiquitously present in several cell types.[18] The bis-POC ester prodrug **10** was prepared by a straightforward S_N2 reaction between a hydroxamate-protected hydroxypiperidinone **7**, the synthetic precursor to **5**, and chloromethyl isopropyl carbonate, followed by palladium-catalyzed hydrogenation of the benzyl moiety. Preparation of the bis-SATE ester prodrug **13** began with acetylation of **5**, which was then activated by thionyl chloride and reacted with *S*-(2-hydroxyethyl) 2,2-dimethylpropanethioate. Hydrolysis of the acetylated hydroxamate yielded **12** (Table 1, compounds **12**). Direct reaction between benzyl precursor **7** and the *S*-(2-hydroxyethyl) 2,2-dimethylpropanethioate was not pursued due to sulfur-derived catalyst poisoning during subsequent hydrogenation. We also synthesized a benzoyloxymethyl (BOM) ester derivative (**11**) in a similar manner to that reported previously, to casually probe the influence of sterics on the efficiency of prodrug hydrolysis.[26] In our in vitro system, treatment with the bis-ester prodrugs resulted in dose-dependent nanomolar IC_{50} values exclusive to D423 cells, which indicated efficient intracellular prodrug hydrolysis (Table 1, compounds **6**−**13**). Among bis-POM, POC, SATE, or BOM prodrugs, the bis-POC prodrug **10** exhibited the lowest IC_{50} value against D423 cells (16 nM), while the bis-SATE prodrug **12** exhibited the highest IC_{50} value against D423 cells (124 nM). Treatment with either bis-POM or bis-BOM prodrugs **6** or **11** resulted in nearly identical IC_{50} values (43 vs 45 nM, respectively). With the exception of the bis-POC prodrug **10**, this set of bis-ester

https://doi.org/10.1021/acs.jmedchem.2c01039
J. Med. Chem. 2022, 65, 13813−13832

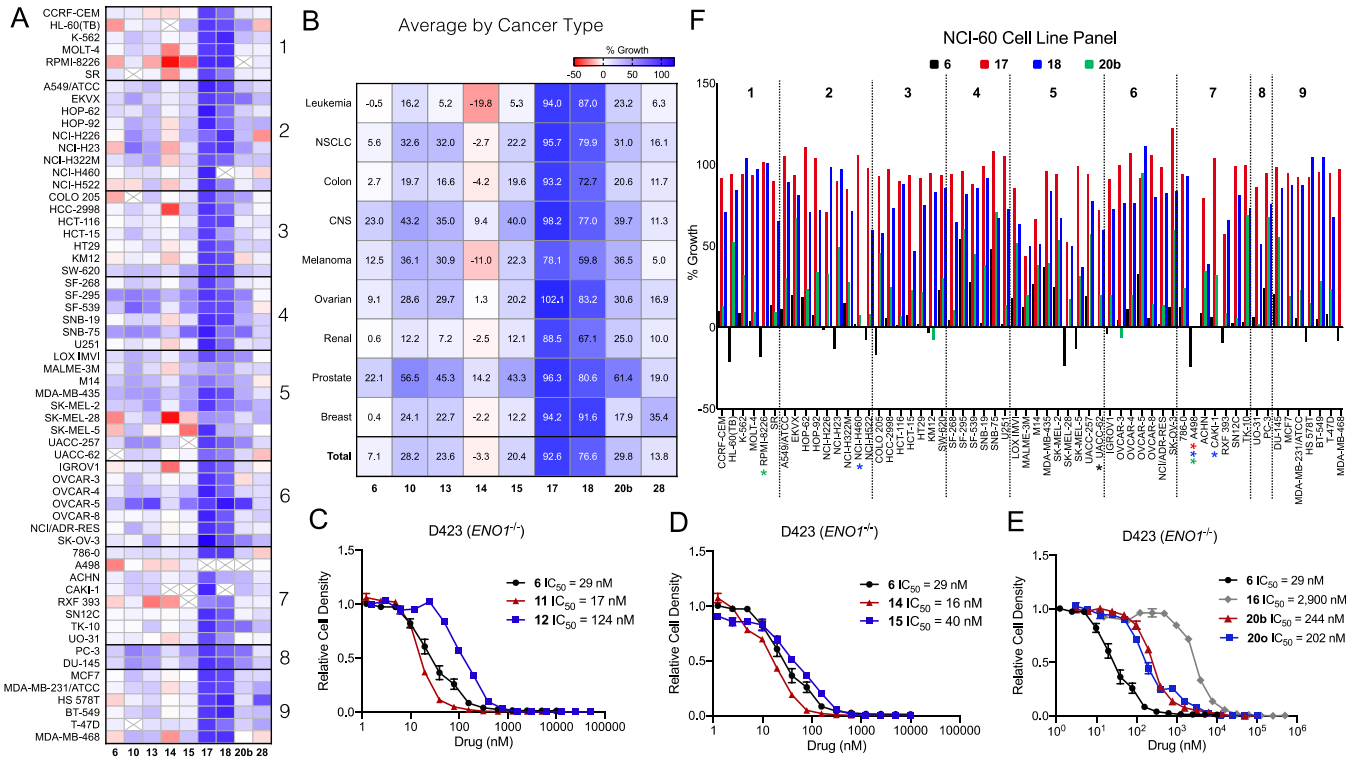

Figure 3. Prodrug identity influences intracellular bioactivation and cytotoxicity of **5**. (A) NCI-60 cell line screening of select prodrugs of **5**. Cells from various cancer subtypes were incubated with 10 μM of prodrug for 24 h and percent growth was measured. Values between 0 and 100% (blue) indicate growth inhibition, while values less than 0% (red) indicate cell killing. (B) Average percent growth per cancer cell subtype for each prodrug. The lipophilic, esterase-labile prodrug **14** consistently yielded the greatest efficacy across all cell lines (total average: −3.3%), while McGuigan prodrugs **17** and **18** consistently yielded the least amount of growth inhibition (total average: +92, +76% growth, respectively). (C) Comparative potency of structurally distinct bis-ester prodrugs of **5** in *ENO1*$^{-/-}$ cells. Treatments with either bis-POM (**6**, black), bis-POC (**11**, red), or bis-SATE (**12**, blue) prodrugs all exhibit potent activity in D423 cells, with observably higher potency achieved by bis-POM or bis-POC prodrugs. (D) Influence of hydroxamate acylation on the potency of **6**. D423 cells were treated with hydroxamate esters of **6** (acetyl, **14**; benzoyl; **15**). The IC_{50} values for **6**, **14**, and **15** are all within the same order-of-magnitude, indicating that acylation of the hydroxamate is generally tolerated. (E) Mono-POM/L-alanine isopropyl ester prodrug **20o** (blue) is efficiently bioactivated to **5** during the 6 day treatment period and exhibits similar activity as mono-POM/benzylamine prodrug **20b** (red). In contrast to the nanomolar potency observed by **6**, **20b**, and **20o**, bis-amidate prodrug **16** (gray) exhibits micromolar activity in D423 cells. Data are presented as the mean ± SEM of $N \geq 2$. (F) Focused view of % growth inhibition for McGuigan prodrugs **17** (red) and **18** (blue) vs bis-POM prodrug **6** (black) and POM/benzylamine prodrug **20b** (green) in the NCI-60 cell line panel. Whereas **6** and **20b** exhibit cytostatic and cytotoxic activity in select cell lines, **17** and **18** are essentially inactive. Asterisks indicate no data for a compound with the corresponding legend color in a cell line. Section numbers correspond to cancer types: 1 = leukemia, 2 = NSCLC, 3 = colon cancer, 4 = CNS cancer, 5 = melanoma, 6 = ovarian cancer, 7 = renal cancer, 8 = prostate cancer, and 9 = breast cancer.

prodrugs generally exhibited similar order-of-magnitude potency. This suggests a high degree of functional group tolerance at the terminal acyl group—the position susceptible to initial (carboxyl)esterase cleavage—which is supported by similar trends in growth inhibition in the NCI-60 cell line screening panel after a 24 h incubation of each prodrug at 10 μM (Figures 3a–c, S4). Similar observations of steric tolerance at the terminal acyl group have also been reported in the SAR studies on the bis-ester prodrug of phosphonate drugs such as adefovir.[15] Closer concordance in growth inhibition between **6** and **13** can likely be explained by the requisite hydrolysis by phosphodiesterases for mono-POM and mono-SATE esters versus the ability for the terminal ester group on mono-POC esters to be cleaved by (carboxyl)esterases—leading to decarboxylation and fragmentation of the second POC promoiety (Figure 2).

With this set of bis-ester prodrugs, we were interested in determining whether esterification of the hydroxamate—thereby further increasing lipophilicity—would increase cellular potency. Similar to the phosphonate esters, we reasoned that the hydroxamate esters would likewise be subject to rapid intracellular cleavage by esterases. We generated the acetyl and benzoyl hydroxamate esters of **6** by simple reaction with the corresponding anhydrides (Scheme 1, compounds **14** and **15**). In our in vitro system, **6**, **14**, and **15** retained selective activity against D423 cells and exhibited similar IC_{50} values (29, 16, and 40 nM, respectively; Table 1, compounds **13**–**15**, Figure 3d). Against the NCI-60 cell line panel, treatment with these hydroxamate ester derivatives **14** and **15** generally resulted in similar trends toward growth inhibition across cell lines as **6**, with some exceptions (11/60 cell lines for **14** and 10/60 cell lines for **15**; Figures 3a,b, S5). These exceptions appear to be cell line-specific as they are not limited to any one cancer subtype and are generally dissimilar between **14** and **15**. The acetylated hydroxamate ester **14** appeared to be removed more efficiently compared to the benzoylated ester **15**, as evidenced by the greater propensity for cell killing in the NCI-60 cell line panel. Compared to **6**, which exhibited an average inhibitory activity of +7.1% across all cell lines, the average growth inhibition by **14** across all cell

https://doi.org/10.1021/acs.jmedchem.2c01039
J. Med. Chem. 2022, 65, 13813−13832

Scheme 2. Phosphonoamidate Prodrugs of 5[a]

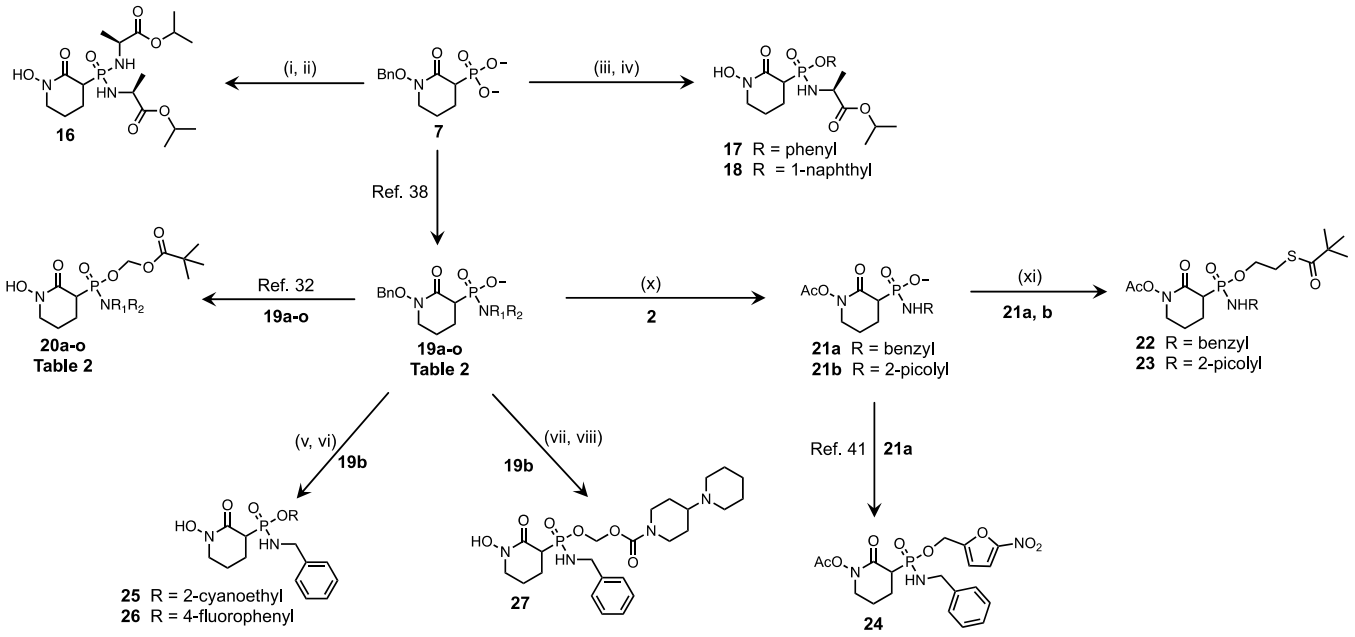

[a]Reagents and conditions: (i) $COCl_2$, cat. DMF, 3 h, then L-alanine isopropyl ester; (ii) H_2, 10% Pd/C, THF/MeOH, 1 h (20−40% yield overall); (iii) $COCl_2$, cat. DMF, 3 h, then L-alanine isopropyl ester, phenol for **17** or 1-naphthol for **18**; (iv) H_2, 10% Pd/C, THF/MeOH, 12 h (30% for **17** and 28% for **18**); (v) $POCl_3$, neat, 30 min, then 2-cyanoethanol for **25** or 4-fluorophenol for **26**; (vi) H_2, 10% Pd/C, THF/MeOH, 1 h (55% for **25** and 42−47% for **26**); (vii) chloromethyl[1,4′-bipiperidine]-1′-carboxylate, chloroform, 2 h, 50 °C; (viii) H_2, 10% Pd/C, THF/MeOH, 2 h (77% overall); (x) H_2, 10% Pd/C, THF/MeOH, 1 h, then Ac_2O/Et_3N neat (70% yield over two steps); (xi) Mitsunobu conditions (see the Experimental Section; 10% for **22** and 15% for **23**).

lines was −3.3% versus +20.4% for **15** (Figure 3b). These data suggest that the low-molecular-weight acetyl ester on **14** is generally more readily removed than the benzoyl ester of **15** across multiple cell lines. Nevertheless, it is also apparent that esterification is generally tolerated on the hydroxamate—as cells treated with low-molecular-weight (acetyl, **14**) or bulkier hydroxamate esters (benzoyl, **15**) yield the same order-of-magnitude IC_{50} values in D423 cells and generally similar trends toward growth inhibition in the NCI-60 cell line panel (Figure 3a,b).

Identification of Aliphatic and Benzylic Amines as Second Promoieties. Next, we synthesized a series of phosphonoamidate prodrugs of **5** (Scheme 2). We first sought to examine two well-established phosphonoamidate strategies: the bis-amidate and McGuigan (ProTide) strategies (Scheme 2, Figure 2).[27−29] Bis-alanyl isopropyl ester prodrug (bis-amidate) **16** was synthesized by chlorination of intermediate **7** followed by coupling with isopropyl L-alaninate and H_2-mediated debenzylation. McGuigan prodrugs **17** and **18** were synthesized by chlorination of **7** followed by sequential addition of phenol or naphthol and isopropyl L-alaninate and then H_2-mediated debenzylation. While rapid intracellular cleavage of the bis-amidate or McGuigan promoieties has been observed for antiviral phosphonate pharmacophores [rabacfosadine, GS-9131, and tenofovir alafenamide (TAF)],[27,28] we did not observe efficient intracellular promoiety removal for either strategy, as evidenced by comparatively high IC_{50} values in D423 cells after 6 day incubation, necessity for longer incubation times to achieve similar order-of-magnitude IC_{50} values as **6**, and inability to substantially curb the growth of any cell line in the NCI-60 cell line screening panel after a 10 μM, 24 h incubation (Table 1, compounds **16**−**18**; Figures 3; S6). Treatment with bis-amidate prodrug **16** in our three-cell line system resulted in dose-dependent, selective toxicity to D423 cells with an IC_{50} value of 2.9 μM; this is approximately 10-fold higher than the values obtained for our bis-ester prodrugs (Table 1). Due to the comparatively weak growth inhibitory data observed for **16**, we examined the effects of increasing the treatment of duration when evaluating the activities of McGuigan prodrugs **17** and **18**. Against D423 cells, 10 day treatment with **17** or **18** yielded IC_{50} values of 18 and 36 nM, respectively (Table 1). Longer drug incubation was required to observe nanomolar cell killing on-par with that observed for the bis-ester prodrugs. Consistent with the slow prodrug bioactivation in our three-cell line system, a single 10 μM incubation of **17** or **18** for 24 h in the NCI-60 cell line panel did not significantly inhibit growth, which contrasts the cytostatic and cytotoxic activities observed by **6** against the same panel (Figures 3a,b, S6). Because both bis-amidate **16** and McGuigan prodrugs **17** and **18** exhibited dose-dependent, selective toxicity of D423 cells in our three-cell line system, the absence of meaningful growth inhibition after a 24 h incubation in the NCI-60 cell line panel suggests inefficient intracellular prodrug removal.

To probe the cause of inefficient prodrug removal on **17** and **18**, we evaluated the stabilities of these compounds in human serum using a ^{31}P NMR-based assay. Whereas bis-POM prodrug **6** was rapidly hydrolyzed to the mono-POM ester intermediate (Figure S3), the prototypical McGuigan prodrug **17** was remarkably stable for over 9 h, as indicated by the presence of a peak at 26 ppm and the absence of any detectable peaks upfield that would suggest hydrolysis (Figures 4b,c; S7). At the 16 h timepoint, we observed the emergence of two peaks at 27.4 and 26.4 ppm, which neighbored the intact peak of **17** at 26.7 ppm; this was accompanied by the faint emergence of a peak at 17 ppm, suggesting hydrolysis of the

https://doi.org/10.1021/acs.jmedchem.2c01039
J. Med. Chem. 2022, 65, 13813−13832

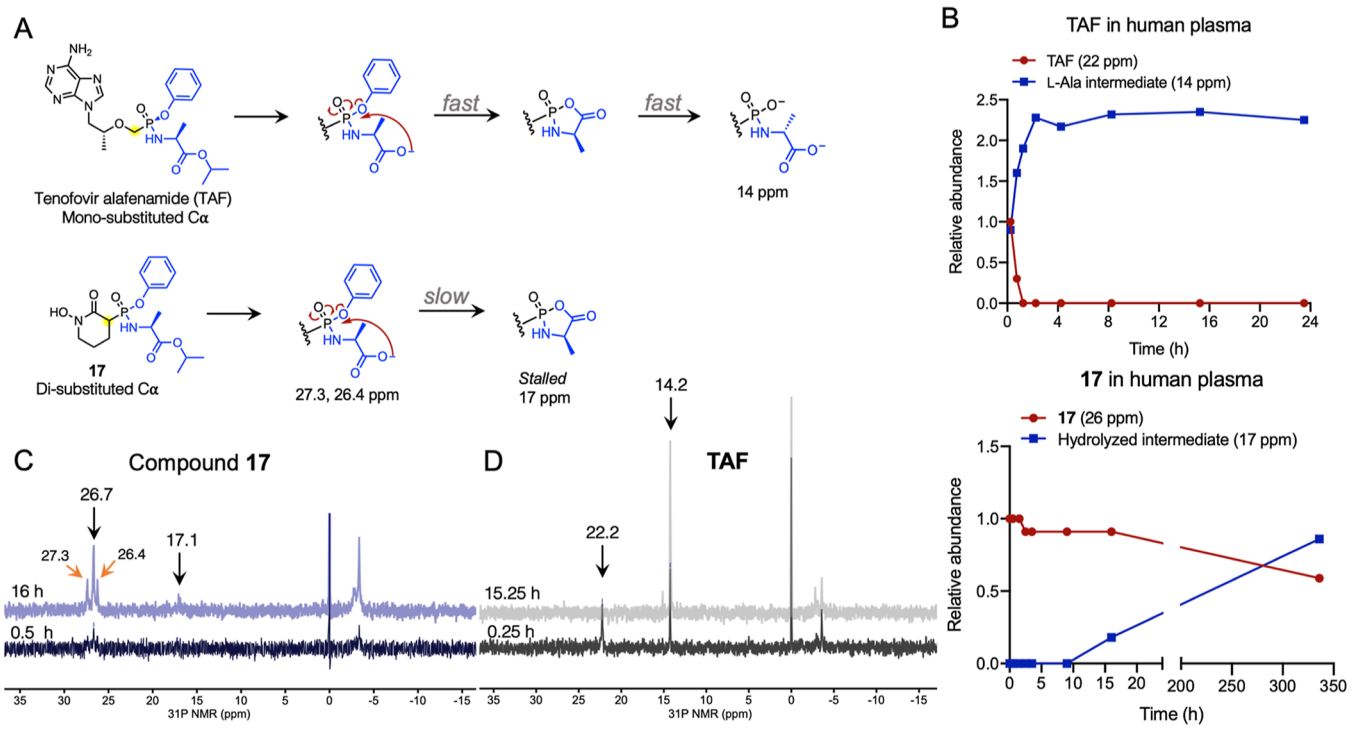

Figure 4. Cα substitution level influences the hydrolysis susceptibility of McGuigan phosphonate prodrugs. (A) TAF and **17** are both McGuigan prodrugs that are bioactivated to their respective phosphonate pharmacophores through a common phosphonoamidate metabolite. (B) Human plasma stability of TAF (2 mM) and **17** (2.5 mM) was measured using a ^{31}P NMR-based assay in 80% human plasma, 20% D_2O. Whereas full hydrolysis of intact TAF (top graph, red trace) to the L-alaninate intermediate (blue trace) occurs rapidly, hydrolysis of intact **17** (bottom, red trace) occurs slowly and is incomplete even after 336 h (14 days). (C) ^{31}P NMR traces from comparable timepoints from stability studies for **17** and (D) TAF in human plasma. In contrast to TAF, for which no intact prodrug is detectable at 15.25 h, intact **17** is still readily detectable at 16 h. At 15.25 h, the only metabolite detected in human plasma is the L-alaninate intermediate present at 14.2 ppm. For **17**, neighboring peaks at 27.3 and 26.4 (orange arrows) correspond to the hydrolyzed isopropyl ester on the alanyl moiety for the *Sp* and *Rp* isomers, respectively.

terminal isopropyl ester to the anionic L-alaninate moiety (Figures 4b,c; S7). The presence of the downfield peaks around 26 ppm falls within the signature region for phosphonoamidate esters, indicating that hydrolysis to the anionic phosphonoamidate intermediate had not fully occurred. By 336 h (14 days), two clear peaks at 16−17 ppm were present, while the downfield peak of intact **17** remained visible but had decreased (Figure S7). That some intact **17** was still present at 336 h, despite the appearance of hydrolysis metabolites, corroborated the inefficient prodrug removal and minimal cytotoxic activity observed in vitro. Inefficient removal of the McGuigan prodrug is likely attributable to the more sterically hindered di-substituted Cα on **5**, which contrasts with the mono-substituted Cα present on TAF and GS-9131 (Figure 4a,b).[28] There is a single report by Dang and co-workers of a higher Cα-substituted McGuigan prodrug on a phosphonic acid-containing thiazole inhibitor of fructose-1,6-bisphosphatase ("compound 35l").[30] While compound 35l was not the focus of their study, the authors noted that this compound was only able to yield modest pharmacodynamic effects in a rat model of type 2 diabetes at a higher dose than for other prodrug strategies they evaluated.[30] This supports the influence of Cα substitution on the efficiency of McGuigan prodrug cleavage as observed on their compound 35l and on our prodrugs **17** and **18**. Additionally, it is well known that McGuigan prodrugs are more rapidly removed in the *Sp* rather than *Rp* configuration.[17,31] While compounds **17** and **18** were evaluated as isomeric mixtures in vitro, the ^{31}P NMR assay allowed for the observation of the hydrolysis susceptibilities of each isomer. In our stability studies, **17** was evaluated as an approximately 1:1 mixture of *Sp* and *Rp* isomers (Figures 4; S7). At the 16 h timepoint, hydrolysis of the isopropyl ester—resulting in the neighboring peaks at 27.4 and 26.4 ppm—occurred at similar rates, as indicated by near-identical peak integrations (Figure 4c). However, at the 336 h timepoint, we observed the concomitant disappearance of the downfield 27.4 ppm peak, appearance of the upfield phosphonoamidate metabolite peaks at approximately 16 ppm, and retention of the peak adjacent to intact **17** (Figure S7). These data indicated that initial hydrolysis of the alkyl ester on the alanyl promoiety can occur in a phosphorous stereochemistry-independent manner. However, the subsequent cyclization and displacement of the phenol moiety likely occurs in a stereochemistry-dependent manner, as only the downfield 27.4 ppm peak decreased concurrently with the appearance of the upfield 16 ppm peaks (Figure S7).

To clarify whether phosphonoamidate prodrugs were, in general, inefficiently cleaved on **5** or whether this was specific to bis-amidate and McGuigan strategies, we synthesized a mono-POM, isopropyl L-alaninate prodrug (**20o**, Table 2) and evaluated this compound in our three-cell line system. The synthesis of phosphonoamidate POM esters **20b−20o** was described previously.[32] Treatment with **20o** for 6 days resulted in dose-dependent, selective toxicity against D423 cells, with an IC_{50} value of 202 nM. Due to the ubiquitous expression of esterases, we reasoned that the order of promoiety removal would first be the POM group followed by the isopropyl L-

https://doi.org/10.1021/acs.jmedchem.2c01039
J. Med. Chem. 2022, 65, 13813−13832

Table 2. SAR of POM Phosphonoamidate Prodrugs of 5[a]

cpd.	R_1	R_2	IC_{50} (nM)			logD[b]
			D423 (*ENO1*$^{-/-}$)	D423 ENO1 (*ENO1*-tg)	LN319 (*ENO1*$^{+/+}$)	
20a	H	H	1,342	307,449	425,512	0.18
20b	H	benzyl	244	3,781	3,394	2.14
20c	H	2-picolyl	97	1,559	1,601	1.06
20d	H	2-flluorobenzyl	202	2,883	9,241	2.28
20e	H	3-fluorbenzyl	258	2,789	2,363	2.28
20f	H	4-fluorobenzyl	136	2,092	1,660	2.28
20g	H	2,4-fluorobenzyl	62	1,637	7,227	2.43
20h	H	2,6-fluorobenzyl	116	1,577	1,410	2.43
20i	H	3,4-fluorobenzyl	227	3,040	3,256	2.43
20j	H	cyclohexane methyl	81	1,189	1,081	2.43
20k	H	cyclopropane methyl	23	470	456	1.17
20l	H	cyclobutyl	120	2,929	2,127	1.27
20m	Me	Me	108	2,184	5,400	0.65
20n	H	Me	63	1,926	12,882	0.41
20o	H	isopropyl L-alanyl	265	2,486	9,942	1.31
20p[c]	H	dodecylamine	2,607	65,725	>100,000	0.45

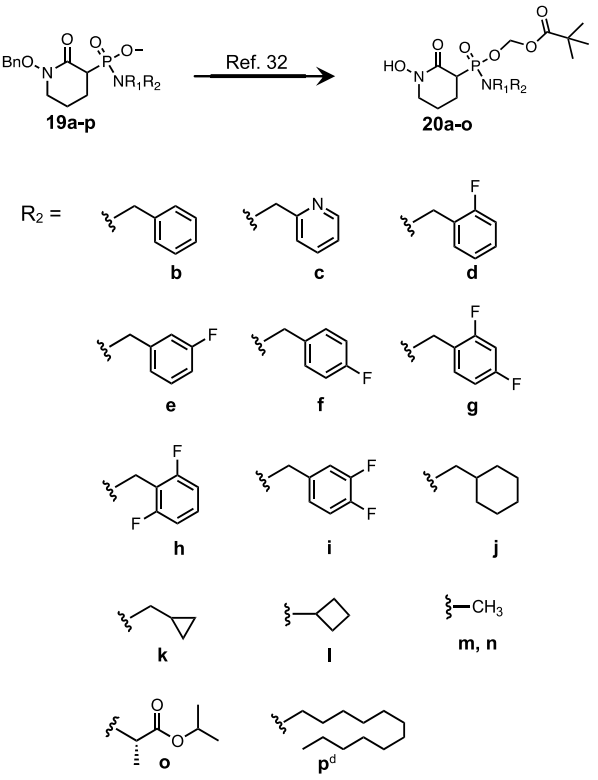

[a]Data are presented as the mean of $N \geq 2$. Full structures are available in the Supporting Information. [b]Values calculated from Chemicalize. [c]Prodrug **20p** contains only dodecylamine and no POM ester.

alaninate. There is extensive literature on the mechanism of amidate hydrolysis on phosphonate- and phosphate-containing nucleotide analogues. Whereas phosphoramidates such as sofosbuvir and remdesivir are mainly cleaved by the histidine nucleotide triad-binding protein 1 (HINT1), phosphonoamidates such as TAF and GS-9191 mainly undergo lysosomal/acid hydrolysis (Figure 4).[31,33−37] By comparing the mechanisms of bioactivation for **20o** and **17** and **18**, we reasoned that the inefficient bioactivation of **17** and **18** likely stems from the requisite intramolecular cyclization step common to McGuigan prodrugs. Compared to other McGuigan phosphonoamidates such as TAF and GS-9131—which both contain a mono-substituted Cα phosphonate—**5** contains a di-substituted Cα phosphonate. Higher-order substitution at Cα on **5** likely impedes both the rate of intramolecular cyclization required to displace the phenol and the subsequent ring-opening hydrolysis. Beyond nucleotide analogues, efficient bioactivation of McGuigan phosphonoamidate prodrugs has also been observed on phospho(no)-antigens containing the phosph(on)ates on mono-substituted Cα, supporting the influence of sterics on the bioactivation of McGuigan prodrugs.[38,39] The proposed causes for inefficient bioactivation are further substantiated by the uniformly poor growth inhibition observed for both **17** and **18** in the NCI-60 cell line panel, which suggests that part of their bioactivation is non-enzymatic and independent of cell line-specific expression of potential phosphonoamidate-hydrolyzing enzymes (Figures 3, S6). The intracellular metabolism of **20o** is distinct from McGuigan prodrugs **17** and **18**, which likely explains the more efficient prodrug bioactivation and the resulting lower IC_{50} value in D423 cells.

The activity of **20o** against D423 cells prompted our exploration into the ability for amines beyond amino acids to serve as second promoieties. Inspired by SAR studies toward the anti-hepatitis C nucleotide prodrug, IDX-184, we first examined the activity of a POM/benzylamine prodrug **20b** in our three-cell line system (Table 2).[32,40] The synthesis of **20b** and this series of amine prodrugs was reported previously.[32] Briefly, phosphonoamidate intermediates were reliably generated using a modified Mitsunobu coupling between benzylated intermediate **7** and the corresponding amine. The POM ester was then appended via direct reaction between phosphonoamidate intermediates, and then palladium-catalyzed hydrogenation yielded the final prodrugs in 60−80% yield over three steps (Table 2). Due to the ubiquity of intracellular esterases, **20b** served as a cell-permeable prodrug to evaluate the efficiency of benzylamine hydrolysis. Treatment with **20b** resulted in dose-dependent, selective toxicity against D423 cells, with an IC_{50} value of 243 nM (Table 2, compound **20b**). We then synthesized and assessed the activities of other POM/benzylic or aliphatic amine prodrugs of **5** in our cell system (Table 2). We observed a high degree of tolerance for the identity of the amine, as indicated by similar order-of-magnitude IC_{50} values for this set of prodrugs. There appeared to be a trend toward increased potency with lower molecular weight aliphatic amines, which may suggest that these promoieties undergo acid hydrolysis more readily—perhaps due to reduced steric or electronic interference (Table 2, compounds **20j−p**). To the best of our knowledge, this was

https://doi.org/10.1021/acs.jmedchem.2c01039
J. Med. Chem. 2022, 65, 13813−13832

the first time non-amino acids were reported to be effective phosphonoamidate promoieties.

Screening First Promoieties with Various Bioactivation Mechanisms. The dianionic nature of **5** at physiological pH warrants attachment of two promoieties to render the molecule neutral. Parallel to our efforts to identify viable second promoieties on **5**, we were also interested in identifying first promoieties that could be applied independently or to any of the phosphonoamidates we had synthesized in Table 2. At the time, we used **21a** or **21b** (or their free hydroxamate counterparts **19b** or **19c**, respectively) as workhorses over other phosphonoamidate intermediates in Table 2 because they were the first for which we had an established synthetic procedure and could readily serve as test compounds to evaluate the feasibility of various first promoiety strategies. We evaluated promoieties with and without a reported precedent—each with various proposed mechanisms of bioactivation. To phosphonoamidate intermediates **21a** or **21b**, we evaluated the efficacies of SATE (IDX-184-like), nitroheterocycle, cyanoethanol, 4-fluorophenol, and [1,4′-bipiperidine]-1′-carboxyl strategies (Table 1, compounds **22**−**27**). The putative mechanisms of the initial mechanism of bioactivation for these prodrugs are, respectively, as follows: esterase (exact identity unknown), hypoxia, alkalinity (based on synthesis approaches for 2-cyanoethanol and 4-fluorophenol), and butyrylcholinesterase.[40−44]

The synthesis of IDX-184-like prodrugs **22** and **23** and alkaline prodrugs **25** and **26** began with either phosphonoamidate intermediates **20b**, **21a**, or **21b**. IDX-like prodrugs **22** and **23** were prepared first by Mitsunobu coupling between either **21b** or **21c** and with *S*-(2-hydroxyethyl) 2,2-dimethylpropanethioate. After purification, the desired products were obtained in approximately 10−15% yield. The synthesis of nitroheterocycle prodrug **24** was previously reported.[41] Alkaline-labile prodrugs **24** and **25** were prepared by monochlorination of intermediate **20b** in neat phosphorous oxychloride for 30 min. We found that neat conditions enabled clean conversion of phosphonoamidate intermediate **20b** to the desired mono-chlorinated product. Attempts to conduct the reaction in standard solvents (chloroform and dichloromethane), with equimolar or excess chlorination reagent, resulted in the formation of several undesired side products, as observed by ^{31}P NMR. Full conversion to the mono-chlorinated product was confirmed by proton-decoupled ^{31}P NMR ($CDCl_3$), which showed a singlet at approximately 35 ppm. For reference, the starting phosphonoamidate has a ^{31}P NMR signal at approximately 22 ppm, and hydroxamate-protected versions of **5** that are dichlorinated display a signal at approximately 45 ppm. The crude reaction mixture was diluted with dichloromethane, and the excess phosphorous oxychloride was removed with aqueous washes (see the Experimental Section). Thereafter, alkaline-labile prodrugs **25** and **26** were synthesized by reacting mono-chlorinated **20b** with either 2-cyanoethanol or 4-fluorophenol, followed by palladium-catalyzed hydrogenation to yield **25** or **26** in approximately 40 and 55% yield, respectively. Finally, butyrylcholinesterase prodrug **27** was synthesized by direct reaction between **20b** and chloromethyl[1,4′-bipiperidine]-1′-carboxylate. Palladium-catalyzed hydrogenation of the benzylated precursor yielded **27** in 77% yield.

Treatment with these phosphonoamidate prodrugs in our three-cell line system yielded varying outcomes. IDX-184-like prodrugs **22** and **23** yielded dose-dependent, selective toxicity in D423 cells with IC_{50} values of 19 and 71 nM, respectively (Table 1). Compared to the POM phosphonoamidate counterparts (Table 2), the higher potency of these mono-SATE prodrugs may suggest slightly more efficient intracellular cleavage of the first ester, perhaps due to the ability for SATE to be cleaved by multiple types of esterases beyond carboxylesterases, such as thioesterases.[45] For nitroheterocycle prodrug **24**, we also observed dose-dependent selective toxicity in D423 cells, with an IC_{50} value of 299 nM (Table 1, compound **24**, 21% O_2).[41] Consistent with previously reported nitroheterocycle prodrugs, imaging agents, and histological stains,[46−48] the activity of **24** improved under hypoxic conditions (1% O_2), yielding an IC_{50} value of 136 nM in D423 cells and lower IC_{50} values in non-target D423 *ENO1* and LN319 cell lines (Table 1, compound **24**: 21% vs 1% O_2). Increased potency under hypoxic conditions across all cell lines concurred with positive control compound TH-302 (evofosfamide) and contrasted with the negative control bis-ester **6** (IC_{50}, 21% O_2 = 79 nM vs IC_{50}, 1% O_2 = 201 nM), supporting the mechanism of bioactivation mediated by the nitroheterocycle prodrug.[41,49] The proposed alkaline-labile prodrug **25** only began exhibiting selective activity in D423 cells above 1 μM, yielding an IC_{50} value of approximately 7 μM after a 6 day treatment; however, the therapeutic index between control cell lines was comparatively low. Our initial interest in 2-cyanoethanol as a potential first promoiety was driven by its use as a base-labile protecting group in oligonucleotide synthesis and the supposition that it was not susceptible to premature plasma esterase hydrolysis.[42,43] We confirmed the human plasma stability of the 2-cyanoethyl promoiety by ^{31}P NMR and ^{1}H−^{31}P heteronuclear single quantum coherence (HSQC) spectroscopy, which possessed high stability but was still biologically labile ($t_{1/2}$ ∼ 10 h, Figure S8).[50,51] That we observed high micromolar, dose-dependent activity against D423 cells compared to control cell lines suggests that the bioactivation of **25** is inefficient but not entirely absent. Derivatives of the 2-cyanoethyl promoiety—perhaps those containing electron-withdrawing groups at the Cα or Cβ—may increase its susceptibility to hydrolysis. In contrast to **25**, 4-fluorophenol phosphonoamidate **26** was inert and did not exhibit meaningful cell killing in our three-cell line system for the duration of the experiment (Table 1). Finally, the irinotecan-like [1,4′-bipiperidine]-1′-carboxyl phosphonoamidate **27** did not exhibit meaningful activity against D423 cells under 15 μM (Table 1).

We also synthesized and evaluated non-phosphonoamidate-based prodrugs of **5**. These included a lipid prodrug **28**, a bis-cyanoethyl prodrug **29**, and salicylic alcohol ("cycloSal") **30** prodrugs (Table 1, entries 19−21). The proposed mechanisms of action for these prodrugs are as follows: phospholipase and alkalinity.[52−55] Lipid prodrug **28** was synthesized by *N*,*N*′-dicyclohexylcarbodiimide coupling between intermediate **7** and 3-(hexadecyloxy)propan-1-ol, followed by the palladium-catalyzed hydrogenation of the product precursor. Lipid prodrug **28** was obtained as an off-white waxy solid in 36% yield. Bis-cyanoethyl prodrug **29** was synthesized by reacting 2-cyanoethanol with dichlorinated **7**, followed by the palladium-catalyzed hydrogenation (72% yield over three steps). Finally, cycloSal prodrug **30** was synthesized by isobutyrylation of **5**, followed by thionyl chloride-mediated dichlorination of intermediate **9** and reaction with salicylic alcohol (39−65% yield over three steps). Treatment with **28** in our three-cell line panel resulted in dose-dependent, selective killing of D423

https://doi.org/10.1021/acs.jmedchem.2c01039
J. Med. Chem. 2022, 65, 13813−13832

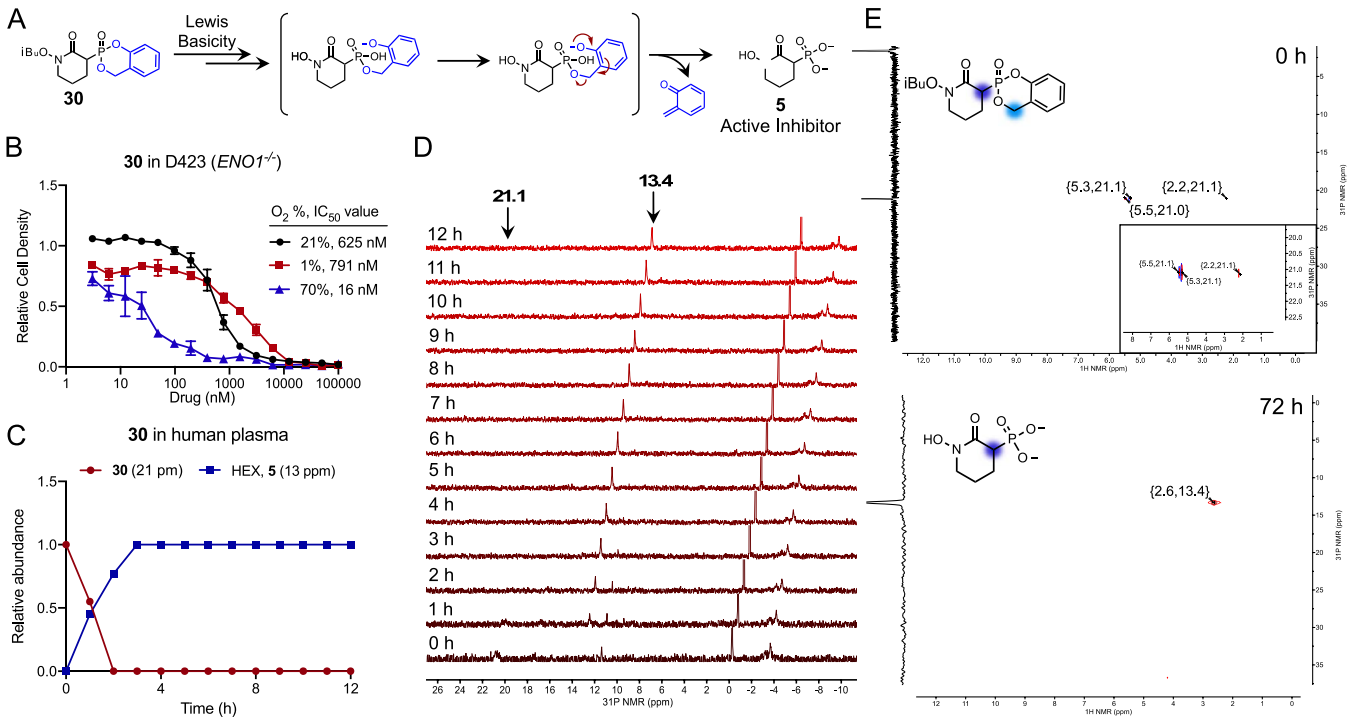

Figure 5. Activity and stability of a cycloSal prodrug of **5**. A cycloSal prodrug of **5** is hydrolyzable under biological conditions. (A) Proposed mechanism of bioactivation of **30**; the 2-(hydroxymethyl)phenol (cycloSal) prodrug is indicated in blue. (B) Activity of **30** in D423 cells at various oxygen levels. While **30** exhibits a slight decrease in potency under hypoxic conditions (red), it is approximately 40-fold more potent under hyperoxic conditions (blue). Across all three conditions, cells were treated with **30** for 6 days. Data are plotted relative to untreated controls and are the mean ± SD of $N \geq 2$. (C) Stability of **30** (2 mM, 1:1 ratio of *Sp* and *Rp* isomers) in 80% human plasma, 20% D_2O as measured by ^{31}P NMR spectroscopy. Peaks were integrated and normalized relative to the phosphate peak at 0 ppm. (D) Time course ^{31}P NMR traces of **30** in human plasma. Intact **30** appears as a broad peak at 21.1 ppm in the human plasma/D_2O solution and is completely hydrolyzed to **5** (13.4 ppm) after 3 h. (E) $^{1}H-^{31}P$ HSQC spectra of intact **30** at time 0 (top) and at 72 h (bottom) with proton resonances on the structure indicated and a focused view of the resonances in the boxed region (top). Top: protons highlighted in light blue correspond to the downfield benzylic protons at 5.3 and 5.5 ppm. The two *x*-axis proton resonances correspond to the broad *y*-axis peak at 21.1 ppm due to the presence of *Sp* and *Rp* isomers. Highlighted in dark blue on the structure is the C*α* proton, which corresponds to the upfield proton resonance at 2.2 ppm. Bottom: hydrolysis of **30** to **5** is complete after 3 h. The 72 h spectrum shows that **5** is the only species detectable in human plasma, as indicated by the C*α* proton resonance at 2.6 ppm, which is highlighted in blue on the structure.

cells, with an IC_{50} value of 207 nM. Lipid prodrug **28** was submitted for further evaluation in the NCI-60 cell line panel, where—with the exception of 13/60 cell lines—it showed a generally similar pattern of activity compared to bis-POM prodrug **6**. The average percent growth across all cell lines treated with **28** was +14% compared to +7% for **6**. For **28**, melanoma cell lines exhibited the lowest overall percent growth after treatment (+5%), which is different than that observed for **6** (Figure 3b). Still, there was considerable variability in percent growth among cell lines within a given cancer type, suggesting differences in the cell line expression of lipase(s) involved in bioactivating **28** to **5**.[56]

Treatment with **29** failed to show activity against any cell line at concentrations up to 100 μM in our in vitro panel (Table 1). Having already observed high micromolar activity of the 2-cyanoethyl/phosphonoamidate prodrug **25** for the same treatment duration, these data with **29** suggest that 2-cyanoethyl phosphonate monoesters are unable to be removed intracellularly. Using a ^{31}P NMR-based assay, we evaluated the stability of **29** in human plasma and found that hydrolysis to the 2-cyanoethyl monoester intermediate occurs with a $t_{1/2}$ of approximately 10 h, while the resulting 2-cyanoethyl monoester intermediate remained intact for the duration of the 35 h experiment (Figure S8). The observation that the first 2-cyanoethyl promoiety can be cleaved under biological conditions supports the dose-dependent killing by **25** and points to the ability for SAR studies to optimize the hydrolytic susceptibility of this promoiety.

Finally, treatment with the alkaline-labile cycloSal prodrug **30** in our three-cell line system resulted in dose-dependent, select toxicity to D423 cells, with an IC_{50} value of 625 nM (Table 1, Figure 5). While this value was higher than that observed for other (esterase-labile) prodrugs, we were pleasantly surprised that **30** appeared to be more readily bioactivated than the other alkaline-labile prodrug, **25**. Prompted by our parallel investigations into the hypoxia dependence of nitroheterocycle prodrug **24**,[41] we also evaluated the O_2-dependent sensitivity of **30** in our three-cell line system (Figure 5b). There appeared to be a slight decrease in potency at 1% O_2 in D423 cells (IC_{50} = 791 nM) and an increase in potency at 70% O_2 (IC_{50} = 16 nM) without a concomitant loss of selectivity after a 6 day treatment course (Figure 5b). While this study is the first to report the O_2-sensitivity of the cycloSal prodrug applied to **5**, a previous report by Sun and colleagues documented the increased potency of the base-labile prodrug temozolomide under hyperoxic conditions in vitro—perhaps supporting a common bioactivation mechanism between the two.[57] We then evaluated the stability of **30** in buffered solutions, culture media, and human serum using a ^{31}P NMR-based assay

https://doi.org/10.1021/acs.jmedchem.2c01039
J. Med. Chem. 2022, 65, 13813−13832

(Figures 5c−e; S10). In contrast to previous reports by Meier on cycloSal prodrugs applied to adefovir, we found that **30** remained intact for at least 3 h at pH 7 (5 mM phosphate buffered D_2O; Figure S10a).[55] In phosphate buffered D_2O pH 7, cycloSal prodrug **30** could be observed for the duration of the 12-h experiment; however, there was some hydrolysis to **5** that emerged at the 12-h timepoint as verified by $^{1}H-^{31}P$ HSQC (Figure S10c). Compared to the low stability of Meier's cycloSal prodrugs of adefovir ($t_{1/2}$ = 0.09 h),[55] the greater stability we observe with **30** could again be attributed to the more substituted nature of Cα on **5**. We then evaluated the stability of **30** in cell culture media and in human serum. Under both conditions, we observed rapid hydrolysis of **30** to the parent **5**, with no intact **30** present at the 3 h timepoint (Figures 5c,d, S10c). We attribute the differences in stability between chemically buffered solutions and biological environments to the presence of nucleophilic protein residues and in situ pK_a effects present in the latter. Given the precedent set by the clinically impactful, alkaline-labile prodrug temozolomide,[58,59] further ongoing work involves evaluating the antineoplastic activity of **30** against intracranial *ENO1*$^{-/-}$ tumors in mice and conducting SAR studies on cycloSal promoiety to improve its biological stability.

CONCLUSIONS

We have synthesized several prodrugs of **5** with various mechanisms of bioactivation and have demonstrated a rapid method for screening prodrug efficiency in our three-cell line system. This is the first report of an expansive prodrug screening on a non-nucleotide phosphonate pharmacophore and is also the first report of a broad prodrug screen on a di-substituted Cα phosphonate. Other instances where phosph(on)ate prodrugs have been evaluated on non-nucleotide analogues include cyclophosphamide, TH-302, fructose 1,6-bisphosphatase inhibitor (MB06322), fosmetpantotenate (RE-024), organophosph(on)ate ligands of the butyrophilin 3A, *N*-acetyl glucosamine, anti-STAT3 phosphotyrosine prodrugs, and fosmidomycin analogues; however, these studies have focused exclusively on either the McGuigan or bis-ester/amidate prodrug strategies.[26,30,38,39,60−63] Most of these studies have also been conducted on phosphates, which exhibit different metabolic susceptibilities compared to phosphonates. By applying precedented and novel prodrug strategies onto **5**, several important insights can be gleaned from this study. First, we have shown that canonical bis-ester prodrugs beyond the POM group exhibit comparable bioactivation efficiencies, as indicated by the selectivity and similar order-of-magnitude IC_{50} values in D423 cells and generally similar trends in growth inhibition in the NCI-60 cell line panel (Figures 3; S4, S6). This concurs with previous reports on nucleotide phosph(on)ates and non-phosph(on)ate prodrugs that are subjected to esterase hydrolysis, supporting the broad substrate scope of (carboxyl)esterases and phosphodiesterases[64,65]

Second, compounds **17** and **18** are the first detailed reports of the McGuigan prodrug strategy applied to a di-substituted Cα phosphonate. Our in vitro results showing inefficient bioactivation of **17** and **18** compared to bis-ester prodrugs of **5** contrast previous studies showing superior bioactivation of McGuigan prodrugs in target cell lines/types—epitomized by pharmacodynamic differences between tenofovir disoproxil and TAF in lymphoid cells.[17,29] Screening **17** and **18** in the NCI-60 cell line panel revealed no significant growth inhibition after a 10 μM incubation for 24 h despite seeing growth-inhibitory activity by their bis-ester counterparts (Figures 3, S6). With the exception of the fructose 1,6-bisphosphatase inhibitor "compound 35l" described by Dang and colleagues, all other reports investigating the McGuigan prodrug strategy have been on mono-substituted Cα phosphonates and, in these cases, efficient bioactivation was observed.[38,39,63,66] Our experience with **17** and **18** further underscores the role of Cα substitution level in modulating the rate of the intramolecular nucleophilic phosphoryl substitution required to displace the phenolic promoiety (Figures 4; S7). It can be reasonably concluded that inefficient bioactivation stems from the intramolecular cyclization step rather than the subsequent ring-opening hydrolysis, based on observations of efficient ring-opening with **30** and previous work by Meier and colleagues on cycloSal and cycloAmb (phosphonoamidate counterparts) prodrugs of adefovir.[55,67]

Third, we have demonstrated the ability for aliphatic amines to serve as second promoieties on phosphonate-containing drugs.[32] In our three-cell line panel, we found that low-molecular-weight aliphatic amines yielded similar—if not slightly superior—drug-releasing ability as benzylic amines, as indicated by the 10-fold lower IC_{50} value and retention of selectivity in D423 cells (Table 2, compound **20b** vs **20n**). These data differ from observations made for the prodrug SAR toward the discovery of IDX-184, in which benzyl amine as a second promoiety exhibited ∼10-fold greater potency compared to *N*-morpholinyl or isopropylamine phosphoramidate derivatives.[40] Such differences can perhaps be explained by the identity of **5**, a phosphonate, versus IDX-184, a phosphate. Previous studies have shown that nucleoside phosphoramidates are susceptible to hydrolysis via HINT1, whereas nucleoside phosphonoamidates are susceptible to hydrolysis under acidic, lyososomal conditions.[34,35] Reduced steric hindrance by low-molecular-weight aliphatic amines could increase the susceptibility of phosphonoamidates to non-enzymatic acid hydrolysis, thereby explaining the order-of-magnitude improved potency observed for **20k** and **20n** compared to **20b** (Table 2, entries 2, 11, and 14). By evaluating the activity of the prototypical cell-permeable phosphonoamidate **20b** against the NCI-60 cell line panel, we observed +30% average overall growth across all cell lines subjected to a 10 μM incubation for 24 h, with some cell lines experiencing growth inhibition (2/60 cell lines: KM12, OVCAR-3; Figures 3a,f; S6). In general, **20b** exhibited intermediate sensitivity against the NCI-60 panel (+30% overall growth) compared to **6** (+7%) and McGuigan prodrugs **17** and **18** (+93, and +77%, respectively; Figure 3b). As **6**, **20b**, **17**, and **18** are all initially susceptible to esterase hydrolysis, differences in sensitivity observed both in our three-cell line panel and in the NCI-60 cell line screening are indicative of differences in second promoiety removal. Comparing percent growth in the NCI-60 panel after treatment with **20b** versus **17** and **18** supports inefficient prodrug removal on the latter. The bioactivations of **20b**, **17**, and **18** all involve carboxylesterases and acid hydrolysis; however, only the McGuigan prodrugs **17** and **18** proceed through an intermediate intramolecular cyclization. The distinctly different average growth inhibition profiles between **20b** and **17** and **18** in the NCI-60 panel (+30% vs +93% and +77%, respectively) thus support the inefficiency of the McGuigan prodrug strategy on higher substituted Cα phosphonates.

Lastly, we identified two non-esterase-labile prodrugs (**28** and **30**) that will be the subjects of further evaluation in vivo.

https://doi.org/10.1021/acs.jmedchem.2c01039
J. Med. Chem. 2022, 65, 13813−13832

Of the prodrug strategies evaluated in vitro, cycloSal prodrug **30** is of particular interest due to its identity as a base-labile prodrug and for its comparatively greater potency against D423 cells than the 2-cyanoethyl prodrug **25**. For GBM purposes, an alkaline-labile prodrug strategy is attractive because of the uniquely sharp pH gradient across the acidic extracellular and alkaline intracellular environments in GBM; this is the basis for cancer specificity of the alkaline-labile prodrug temozolomide, the only FDA-approved drug with demonstrated activity in GBM.[68−70] Further studies will focus on derivatization of the cycloSal promoiety, including the synthesis of phosphonoamidate cycloAmb prodrugs of **5**, to improve the plasma stability of this prodrug class.[55]

In summary, we have synthesized and evaluated the activities of several canonical and novel prodrug strategies on a small molecule phosphonate inhibitor of ENO2 for the treatment of *ENO1*$^{-/-}$ cancers. In addition to narrowing the scope of prodrug directions for our work with **5**, our data also provide insight into the utility of established phosphonate prodrug strategies on a structurally distinct, non-nucleotide pharmacophore. Using the NCI-60 cell line screening panel, we have illustrated the influence of cell line-dependent enzyme expression on prodrug bioactivation and have demonstrated the utility of this resource for examining prodrug/cell line sensitivity relationships; this will be the subject of further studies by our group as it pertains to **5**. One limitation of the NCI-60 data is the inability to discern whether cytotoxicity is driven by prodrug bioactivation efficiency or cell line-specific sensitivity to enolase inhibition. Still, in conjunction with other corroborative studies presented here, the NCI-60 cell line screen is a useful tool to broadly gauge cell line/prodrug bioactivation susceptibilities. Ultimately, the results from this study have narrowed the scope of prodrugs that will be further explored by our group and may also provide inspiration for prodrug development studies on other phosph(on)ate-containing drugs by others.

EXPERIMENTAL SECTION

All prodrugs were initially synthesized and characterized at MD Anderson Cancer Center. Commercially available solvents and reagents were purchased at the highest available purity and used without further purification. Nuclear magnetic resonance (NMR) spectra were recorded on a Bruker AVANCE III 600, 500 MHz, 400 MHz, or 300 MHz spectrometer as indicated. Proton and phosphorous NMR spectra are reported in parts per million (ppm) on the δ scale; proton NMR spectra are referenced from the residual protium in the indicated NMR solvent ($CDCl_3$, δ 7.24; D_2O, δ 4.80; MeOD, δ 4.78). Data are reported as follows: chemical shift [multiplicity (s = singlet, d = doublet, t = triplet, q = quartet, m = multiplet, dt = doublet of triplets br = broad); coupling constants (J) in hertz; integration. Phosphorus-31 NMR spectra were obtained using the composite pulse decoupling sequence (^{31}P CPD) and are reported as such. Final compounds were purified using a reverse-phase high-performance liquid chromatograph (Agilent G1361A 1260 Infinity) using a stepwise gradient (1−60% buffer B over 25 min, 60−100% buffer B over 10 min, 100% buffer B over 5 min, 100−0% buffer B over 1 min; buffer A: dH_2O with 0.1% TFA, buffer B: MeCN + 0.1% TFA), unless otherwise noted. Purity of final compounds was determined by NMR spectroscopy and/or HPLC and was >95% unless otherwise noted. Liquid chromatography−mass spectrometry (MS) was conducted using either a Waters H class ultra-performance liquid chromatograph with a Waters Acquity UPLC BEH C18 1.7 μm, 2.1 mm × 50 mm column, UV detection between 200 and 400 nm, evaporating light scattering detection, and a SQ detector mass spectrometer with ESI or a Water I class ultra-performance liquid chromatograph with a Waters Acquity UPLC CSH C18 1.7 μm, 2.1 mm × 50 mm column, UV detection at 254 and 290 nm, evaporating light scattering detection, and a SQ detector 2 mass spectrometer with ESI. The injection volume was 5 μL. Chromatographic separation was performed on a Waters Acquity UPLC BEH C18 1.7 μm, 2.1 mm × 50 mm column at a flow rate of 0.5 mL/min. The mobile phases were 0.1% acetic acid in water (solvent A) and 0.1% acetic acid in acetonitrile (solvent B). The gradient had a total run time of 3 min (A/B: a = 10−95% MeCN/water mixture, b = 0.1% formic acid in water, 0−3 min). The column temperature was kept at 40 °C. The samples were analyzed using the positive ESI mode. The ESI source temperature was set at 375 °C, the capillary temperature at 320 °C, and the electrospray voltage at 4.1 kV. Sheath and auxiliary gases were of 45 arbitrary unit and 10 arbitrary unit, respectively. Physiochemical properties of prodrugs were obtained from Chemicalize and are expressed at pH 7.4.

The syntheses of **6**, **7**, **14**, **15**, **16**, **20a−p**, and **24** have been reported previously.[12,13,32,41] Spectra for new compounds are provided in the Supporting Information.

(((1-Hydroxy-2-oxopiperidin-3-yl)phosphoryl)bis(oxy))bis-(methylene) Diisopropyl Bis(carbonate) (10). To a solution of 1-((benzyloxy)-2-oxopiperidin-3-yl)phosphonic acid **7** (50 mg, 176 μmol) in MeCN (1 mL), chloromethyl isopropyl carbonate (48.8 μL, 351.8 μmol) and triethylamine (12.3 μL, 88.0 mol) were added and allowed to stir at 50 °C for 3 h. The reaction was concentrated under reduced pressure, resuspended in CH_2Cl_2, and sequentially washed with 1 volume of the following aqueous solutions: water, 1 M HCl, 1 M saturated $NaHCO_3$, and brine. The organic layer was dried over sodium sulfate, filtered, and concentrated under reduced pressure to a pale-yellow oil and lyophilized for 12 h. The oil was used without further purification and resuspended in a 1:1 solution of tetrahydrofuran (THF)/MeOH. Separately, a mixture of the 10% palladium on carbon in a 3:2 solution of THF/MeOH (5 mL) was prepared and incubated under 15 psi of H_2 for 1 h. Thereafter, the solution containing the benzylated precursor, (((1-hydroxy-2-oxopiperidin-3-yl)phosphoryl)bis(oxy))bis(methylene) diisopropyl bis(carbonate), was added to the mixture and was reacted under 15 psi of H_2 1 for h. The crude reaction was filtered, concentrated under reduced pressure, and purified via reverse-phase HPLC. Lyophilization occurred to afforded **10** as a white solid (49 mg, 69% overall). ^{1}H NMR (600 MHz, $CDCl_3$) 8.24 (s, 1H), 5.77 (q, J = 7.8, 5.4, 5.4 Hz, 2H), 5.73 (t, J = 6.7, 7.7 Hz, 2H), 4.94 (m, 2H), 3.65 (m, 2H), 3.17 (dt, J = 27.9 Hz, 1H), 2.25 (m, 1H), 2.15 (m, 2H), 1.92 (m, 1H), 1.31−1.34 (m, 12H). ^{13}C NMR (151 MHz, $CDCl_3$) 160.01 (d, 4.66 Hz), 153.18, 153.16, 85.12 (d, 5.5 Hz), 84.31 (d, 5.9 Hz), 73.12 (d, 16.63 Hz), 49.73 (s, 2C), 41.51 (d, 143.68 Hz), 22.11 (d, 3.64 Hz), 21.71 (d, 11.6 Hz), 21.63 (s, 4C). ^{31}P NMR (243 MHz, $CDCl_3$) 22.85. Analysis by ESI$^+$ (expected $[M + H]^+$ = 428.34. Observed $[M + H]^+$ = 428.32).

(((1-Hydroxy-2-oxopiperidin-3-yl)phosphoryl)bis(oxy))bis-(methylene)dibenzoate (11). To a solution of 1-((benzyloxy)-2-oxopiperidin-3-yl)phosphonic acid **7** (50 mg, 176 μmol) in MeCN (1 mL), chloromethyl benzoate (60 mg, 351.8 μmol) and triethylamine (12.3 μL, 88.0 mol) were added and allowed to stir at 50 °C for 3 h. The reaction was concentrated under reduced pressure, resuspended in CH_2Cl_2, and sequentially washed with 1 volume of the following aqueous solutions: water, 1 M HCl, 1 M saturated $NaHCO_3$, and brine. The organic layer was dried over sodium sulfate, filtered, and concentrated under reduced pressure to a pale-yellow oil and lyophilized for 12 h. The oil was then resuspended in THF/MeOH (5 mL). Separately, a mixture of the 10% palladium on carbon in a 3:2 solution of THF/MeOH was prepared and incubated under 15 psi of H_2 for 1 h. Thereafter, the solution containing the benzylated precursor, (((1-(benzyloxy)-2-oxopiperidin-3-yl)phosphoryl)bis-(oxy))bis(methylene) dibenzoate, was added to the mixture and was reacted under 15 psi of H_2 for 1 h. The crude reaction was filtered, concentrated under reduced pressure, purified via reverse-phase HPLC. Lyophilization afforded **11** as a white solid (52 mg, 64% overall). ^{1}H NMR (500 MHz, $CDCl_3$): δ 8.02 (dd, J = 28.06 Hz, 4H), 7.56 (m, 2H), 7.43 (m, 4H), 6.05 (m, 2H), 5.93 (d, J = 13.14 Hz,

https://doi.org/10.1021/acs.jmedchem.2c01039
J. Med. Chem. 2022, 65, 13813−13832

2H), 3.60 (m, 2H), 3.23 (dt, J = 25.95 Hz, 1H), 2.12 (m, 3H), 1.85 (m, 1H). ^{31}P NMR (202 MHz, $CDCl_3$): δ 23.72 (s, 1P). Analysis by ESI$^+$ (expected $[M + H]^+$ = 464.38. observed $[M + H]^+$ = 464.43).

S,S′-((((1-Hydroxy-2-oxopiperidin-3-yl)phosphoryl)bis(oxy))bis(ethane-2,1-diyl))bis(2,2-dimethylpropanethioate) (12). To a solution of **13** (100 mg, 190.2 μmol) in MeCN, Cs_2CO_3 (6.20 mg, 19.03 μmol) was added. The reaction was allowed to stir at room temperature for 10 min and was monitored by UPLC−MS. Then, the reaction mixture was concentrated under reduced pressure and re-dissolved in CH_2Cl_2. Next, the organic layer was washed sequentially with 1 volume of the following aqueous washes: water, 1 M HCl, saturated sodium bicarbonate, brine, and water. The organic layer was isolated, dried over sodium sulfate, and concentrated under reduced pressure to a clear oil. The washed produced was then purified via reverse-phase HPLC to yield **12** as a clear oil (38 mg, 41%). ^{1}H NMR (500 MHz, $CDCl_3$): δ 9.85 (s, 1H), 4.06−4.27 (m, 4H), 3.31−3.43 (m, 2H), 3.10 (q, J = 7.01 Hz, 4H), 3.04 (dt, J = 26.35 Hz, J = 7.06 Hz, 1H), 1.79−1.90 (m, 1H), 1.70−1.76 (m, 1H), 1.62−1.69 (m, 1H), 1.51−1.58 (m, 1H), 1.17 (s, 18H). ^{13}C NMR (125 MHz, $CDCl_3$): δ 205.78 (s, 2C), 157.44 (s, 1C), 65.11 (d, J = 119.36 Hz, 2C), 48.42 (s, 1C), 46.55 (s, 2C), 51.40 (d, J = 418.12 Hz, 1C), 28.87 (d, J = 19.2 Hz, 2C), 27.32 (m, 6C), 22.66 (d, J = 4.59 Hz, 1C), 21.29 (d, J = 8.53 Hz, 1C). ^{31}P NMR (202.4 MHz, $CDCl_3$): δ 23.64 (s, 1P). Analysis by ESI$^+$ (expected $[M + H]^+$ = 484.57. Observed $[M + H]^+$ = 484.52).

3-(Bis(2-(pivaloylthio)ethoxy)phosphoryl)-2-oxopiperidin-1-yl Acetate (13). To a solution of **5** (515 mg, 2.64 mmol) in neat acetic anhydride (3 mL), triethylamine (552 μL, 3.96 mmol) was added, and the reaction was allowed to proceed with end-over-end rotation for 12 h. Reaction progress was monitored by UPLC−MS. The reaction was quenched with the addition of 1 volume of CH_2Cl_2 and concentrated under reduced pressure. The resulting orange oil was resuspended in water (5 mL), and the aqueous layer was washed 3 times with 1 volume of CH_2Cl_2. The aqueous layer was isolated and **8** was lyophilized to an orange oil. Next, to a solution of **8** (348 mg, 1.25 mmol) in CH_2Cl_2 (5 mL), *S*-(2-hydroxyethyl) 2,2-dimethylpropanethioate (505 μL, 3.12 mmol), triphenyl phosphine (654 mg, 2.29 mmol), and diisopropyl azodicarboxylate (489 μL, 2.49 mmol) were added sequentially. The reaction was allowed to proceed for 12 h and was monitored by UPLC−MS. Then, the crude product was washed sequentially with 1 volume of the following aqueous solutions: water, brine, and water. The organic layer was isolated, dried over sodium sulfate, and concentrated under reduced pressure to an orange oil. The crude product was then purified by reverse-phase HPLC. Lyophilization yielded **13** as a clear oil (66 mg, 10% overall). ^{1}H NMR (500 MHz, $CDCl_3$): δ 4.26 (m, 2H), 4.15 (m, 2H), 3.68 (m, 1H), 3.60 (m, 1H), 3.17 (dt, J = 18.20 Hz, 1H), 3.13 (t, J = 6.31, 6.40 Hz, 4H), 2.30 (m, 1H), 2.16 (s, 3H), 1.97 (m, 1H), 1.19 (d, J = 1.71 Hz, 18H). Note: some aliphatic ring protons were hidden under the acetyl ester proton peak at 2.18 ppm; alpha proton was partially hidden under the triplet at 3.13 ppm. ^{13}C NMR (125 MHz, $CDCl_3$): δ 205.68 (s, 2C), 161.08 (d, J = 5.02 Hz, 1C), 65.89 (d, J = 7.03 Hz, 1C), 64.93 (d, J = 6.82 Hz, 1C), 51.28 (s, 2C), 46.49 (s, 1C), 42.60 (d, J = 70.41 Hz, 1C), 28.90 (s, 1C), 28.72 (s. 1C), 27.31 (s, 6C), 22.62 (d, J = 4.31 Hz, 1C), 22.02 (d, J = 8.81 Hz, 1C), 18.24 (s, 1C). ^{31}P NMR (202 MHz, $CDCl_3$): δ 23.16 (s, 1P). Analysis by ESI$^+$ (expected $[M + H]^+$ = 526.61. Observed $[M + H]^+$ = 526.48).

Isopropyl((1-hydroxy-2-oxopiperidin-3-yl)(phenoxy)-phosphoryl)-L-alaninate (17). (1-(Benzyloxy)-2-oxopiperidin-3-yl)phosphonic acid **7** (52 mg, 183 μmol) was added to anhydrous CH_2Cl_2 (2 mL) with a catalytic amount of anhydrous dimethylformamide (DMF). To this mixture was added oxalyl chloride (300 μL of a 2.0 M solution in CH_2Cl_2, 547 μmol). The reaction mixture was allowed to stir at ambient temperature for 1 h. Reaction progress was monitored using ^{31}P NMR spectroscopy by observing the appearance of a peak at 44 ppm and the disappearance of the peak at 20 ppm. The reaction mixture was concentrated under reduced pressure, and the dense yellow oil was further lyophilized for 2 h to provide (1-(benzyloxy)-2-oxopiperidin-3-yl)phosphonic dichloride, which was used without further purification. Separately, L-alaninate isopropyl ester hydrochloride salt was azeotroped with anhydrous toluene (0.2 mL × 2) and lyophilized for 12 h. Then, to a solution of phenol (13 mg, 140 μmol) in anhydrous CH_2Cl_2 (3 mL), triethylamine (100 μL, 600 μmol) was added, and the mixture was cooled on dry ice for 15 min. The prepared dichloride was dissolved in anhydrous CH_2Cl_2 (3 mL) and added dropwise over 5 min to the phenol solution. Reaction progress was monitored via UPLC−MS. After 15 min, a solution of isopropyl L-alaninate hydrochloride in anhydrous CH_2Cl_2 (3 mL) was added. The mixture was allowed to warm to ambient temperature and stirred for 12 h. Reaction progress was monitored via UPLC−MS. Then, the reaction mixture was diluted with CH_2Cl_2 (10 mL). The mixture was washed sequentially with 1 volume of water, and the organic layer was isolated and washed with 1 volume of brine, dried over sodium sulfate, and concentrated under reduced pressure to give crude isopropyl((1-(benzyloxy)-2-oxopiperidin-3-yl)(phenoxy)-phosphoryl)-L-alaninate as a brown oil, which was used without further purification (26 mg, 33%). To a mixture of THF/MeOH (1:1 solution, 4 mL) and 10% Pd/C (50 mg), benzylated precursor, isopropyl((1-(benzyloxy)-2-oxopiperidin-3-yl)(phenoxy)-phosphoryl)-L-alaninate, was added. The mixture was hydrogenated at atmospheric pressure and ambient temperature for 12 h. The crude reaction mixture was filtered and concentrated under reduced pressure. The crude mixture was resuspended in CH_2Cl_2 (10 mL) and sequentially washed with 1 volume of water and brine. The organic layer was isolated and dried over sodium sulfate and concentrated under reduced pressure to afford **17** as a light brown oil (19 mg, 30% yield overall). ^{1}H NMR: (400 MHz DMSO-d_6): δ 9.83−9.71 (m, 1H), 7.3−7.12 (m, 5H), 5.27−5.18 (m, 1H), 4.89−4.80 (m, 1H), 3.95−3.90 (m, 1H), 3.51−3.50 (br, J = 4.5 Hz, 2H), 3.34−3.22 (m, 1H), 2.06−1.78 (m, 4H), 1.24−1.06 (m, 9H) ^{31}P NMR (202 MHz, $CDCl_3$) 29.1 (s, 1P), 26.5 (s, 1P) *isomers*. Analysis by ESI$^+$ (expected $[M + H]^+$ = 385.3. Observed $[M + H]^+$ = 385.0).

Isopropyl((1-hydroxy-2-oxopiperidin-3-yl)(naphthalen-1-yloxy)phosphoryl)-L-alaninate (18). 1-((Benzyloxy)-2-oxopiperidin-3-yl)phosphonic acid **7** (50 mg, 176 μmol) was added to anhydrous CH_2Cl_2 (2 mL) with a catalytic amount of anhydrous DMF. To this mixture was added oxalyl chloride (300 μL of a 2.0 M solution in CH_2Cl_2, 547 μmol). The reaction mixture was allowed to stir at ambient temperature for 1 h. Reaction progress was monitored using ^{31}P NMR by observing the appearance of a peak at 44 ppm and the disappearance of the peak at 20 ppm. The reaction mixture was concentrated under reduced pressure, and the dense yellow oil was further lyophilized for 2 h to provide (1-(benzyloxy)-2-oxopiperidin-3-yl)phosphonic dichloride, which was used without further purification. Separately, L-alaninate isopropyl ester hydrochloride salt was azeotroped with anhydrous toluene (0.2 mL × 2) and lyophilized for 12 h. Then, to a solution of 1-naphthol (20.3 μL, 155 μmol) in anhydrous CH_2Cl_2 (3 mL), triethylamine (100 μL, 0.6 mmol) was added, and the mixture was cooled on dry ice for 15 min. The prepared dichloride was dissolved in anhydrous CH_2Cl_2 (3 mL) and added dropwise over 5 min to the phenol solution. Reaction progress was monitored via UPLC−MS. After 15 min, a solution of isopropyl L-alaninate hydrochloride in anhydrous CH_2Cl_2 (3 mL) was added. The mixture was allowed to warm to ambient temperature and stirred for 12 h. Reaction progress was monitored using UPLC. Then, the reaction mixture was diluted with CH_2Cl_2 (10 mL). The mixture was washed sequentially with 1 volume of water, and the organic layer was isolated and washed with 1 volume of brine, dried over sodium sulfate, and concentrated under reduced pressure to give crude isopropyl((1-(benzyloxy)-2-oxopiperidin-3-yl)(phenoxy)-phosphoryl)-L-alaninate as a brown oil, which was used without further purification (21 mg, 29%). To a mixture of THF/MeOH (1:1 solution, 4 mL) and 10% Pd/C (50 mg), benzylated precursor, isopropyl((1-(benzyloxy)-2-oxopiperidin-3-yl)(naphthalen-2-yloxy)-phosphoryl)-L-alaninate, was added. The mixture was hydrogenated at atmospheric pressure and ambient temperature for 12 h. The crude reaction mixture was filtered and concentrated under reduced pressure. The crude mixture was resuspended in CH_2Cl_2 (10 mL) and sequentially washed with 1 volume of water and brine. The organic layer was isolated and dried over sodium sulfate and

https://doi.org/10.1021/acs.jmedchem.2c01039
J. Med. Chem. 2022, 65, 13813−13832

concentrated under reduced pressure to afford **18** as a light brown oil (17 mg, 28% yield overall). ^{1}H NMR (500 MHz, $CDCl_3$): δ 8.20 (d, J = 8.29 Hz, 1H), 7.79 (d, J = 7.79 Hz, 1H), 7.62 (d, J = 4.57 Hz, 1H), 7.45 (m, 4H), 4.82 (m, 1H), 4.67 (m, 1H), 3.46, (m, 2H), 3.23 (m, 1H), 2.26 (m, 3H), 2.12 (m, 1H), 1.97 (m, 1H), 0.93 (d, J = 3.27 Hz, 3H), 0.83 (d, J = 3.51 Hz, 6H). ^{31}P NMR (202 MHz, $CDCl_3$): δ 25.62 (s, 1P), 24.26 (s, 1P) *isomers*. Analysis by ESI$^+$ (expected $[M + H]^+$ = 435.4. Observed $[M + H]^+$ = 435.4).

3-((Benzylamino)(2-(pivaloylthio)ethoxy)phosphoryl)-2-oxopiperidin-1-yl Acetate (22). To a solution of intermediate **21a** (92 mg, 282 μmol) in anhydrous chloroform (4 mL), *S*-(2-hydroxyethyl) 2,2-dimethylpropanethioate (68.6 μL, 422.9 μmol), triphenyl phosphine (110.9 mg, 422.9 μmol), and diisopropyl azodicarboxylate (83.0 μL, 422.9 μmol) were added. The reaction was stirred at ambient temperature for 30 min. Then, the crude reaction was washed with 1 volume of water. The organic layer was isolated and concentrated under reduced pressure, purified by reverse-phase HPLC, and lyophilized to yield **22** as a colorless oil (2.2 mg, 10%). ^{1}H NMR (500 MHz, $CDCl_3$): δ 7.32 (m, 5H), 4.25 (m, 2H), 4.05 (m, 2H), 3.63 (t, J = 5.67, 6.44 Hz, 2H), 3.22 (dt, J = 24.39 Hz, 1H), 3.08 (t, J = 6.68, 6.92 Hz, 2H), 2.18 (s, 3H), 2.12 (m, 1H), 1.99 (m, 1H), 1.20 (d, J = 3.94 Hz, 9H). Note: some aliphatic ring protons were hidden under the acetyl ester proton peak at 2.18 ppm. ^{31}P NMR (202 MHz, $CDCl_3$): δ 28.88 (s, 1P), 28.77 (s, 1P) *isomers*. Analysis by ESI$^+$ (expected $[M + H]^+$ = 471.52. Observed $[M + H]^+$ = 471.42).

2-Oxo-3-((2-(pivaloylthio)ethoxy)((pyridin-2-ylmethyl)amino)phosphoryl)piperidin-1-yl Acetate (23). To a solution of intermediate **21b** (300 mg, 916.7 μmol) in anhydrous CH_2Cl_2 (12 mL), *S*-(2-hydroxyethyl) 2,2-dimethylpropanethioate (220.9 μL, 1.37 mmol), triphenyl phosphine (360.7 mg, 1.37 mmol), and diisopropyl azodicarboxylate (267.3 μL, 1.37 mmol) were added. The reaction was stirred at ambient temperature for 12 h, and reaction progress was monitored by ^{31}P NMR spectroscopy. Then, the crude reaction was washed with 1 volume of water. The organic layer was isolated and concentrated under reduced pressure, purified by reverse-phase HPLC, and lyophilized to yield **23** as a colorless oil (65 mg, 15%). ^{1}H NMR (500 MHz, $CDCl_3$): δ 8.75 (d, J = 5.51 Hz, 1H), 8.11 (t, J = 7.43, 8.03, 1H), 7.83 (d, J = 8.03 Hz, 1H), 7.56 (t, J = 6.47, 6.47 Hz, 1H), 4.97 (q, J = 8.72, 8.94, 9.42 Hz, 1H), 4.65 (d, J = 12.62 Hz, 2H), 4.02 (m, 2H), 3.61 (m, 2H), 3.24 (dt, J = 24.07 Hz, 1H), 2.33 (m, 1H), 2.17 (s, 3H), 1.20 (s, 9H). Note: some aliphatic ring protons were hidden under the acetyl ester proton peak at 2.18 ppm. ^{31}P NMR (202 MHz, $CDCl_3$): δ 28.28 (s, 1P), 28.16 (s, 1P) *isomers*. Analysis by ESI$^+$ (expected $[M + H]^+$ = 472.52. Observed $[M + H]^+$ = 472.44).

Cyanomethyl *N*-Benzyl-*P*-(1-hydroxy-2-oxopiperidin-3-yl)-phosphonamidate (25). Intermediate **19b** (50 mg, 133.9 μmol) was dissolved in neat phosphorous oxychloride (2 mL) at 0 °C and was allowed to react for 30 min. Reaction progress was monitored by ^{31}P NMR spectroscopy and was determined to be complete by the formation of a peak at approximately 32 ppm corresponding to the monochlorinated product. Next, the reaction was diluted with 1 volume of anhydrous CH_2Cl_2 and concentrated under reduced pressure to a colorless oil. The crude product was redissolved in anhydrous CH_2Cl_2 (4 mL) and washed sequentially with 0.5 volumes of the following aqueous solutions: water (3×), saturated $NaHCO_3$, water, brine, and water. The organic layer was isolated and concentrated under reduced pressure to a colorless oil. The washed product was then redissolved in anhydrous CH_2Cl_2 (3 mL) and cooled to −78 °C under argon. Separately, 2-cyanoethanol (17.6 μL, 254.6 μmol) was dissolved in anhydrous CH_2Cl_2 (1 mL), and this was then added dropwise to the main reaction vessel. The reaction was allowed to proceed for 2 h from −78 °C to ambient temperature. Thereafter, the reaction was heated at 50 °C for 30 min. Reaction progress was monitored by ^{31}P NMR and ^{1}H−^{31}P HSQC spectroscopy by the emergence of two peaks at approximately 30−32 ppm. The crude reaction was then washed sequentially with 1 volume of the following aqueous solutions: 1 M HCl, saturated $NaHCO_3$, and brine. The organic layer was isolated and concentrated under reduced pressure to yield the benzylated intermediate 2-cyanoethyl *N*-benzyl-*P*-(1-(benzyloxy)-2-oxopiperidin-3-yl)phosphonamidate as a colorless oil; this was lyophilized for 12 h. Then, a mixture of 10% palladium on carbon was added to MeOH (4 mL) and was pre-saturated with a balloon of H_2 for 1 h. Separately, the benzylated intermediate 2-cyanoethyl *N*-benzyl-*P*-(1-(benzyloxy)-2-oxopiperidin-3-yl)-phosphonamidate was dissolved in MeOH (2 mL), which was then added to the main reaction vessel. The hydrogenation reaction was allowed to proceed for 1 h. Reaction progress was monitored by UPLC−MS and $FeCl_3$ staining on thin-layer chromatography. The reaction was then concentrated under reduced pressure, purified by reverse-phase HPLC, and lyophilized to yield **25** as a colorless oil (17 mg, 55% overall). ^{1}H NMR (500 MHz, $CDCl_3$): δ 7.25 (m, 5H), 4.34 (m, 1H), 4.19 (d, J = 13.69, 2H), 3.90 (m, 2H), 3.53 (t, J = 5.82, 6.62 Hz, 2H), 3.02 (dt, J = 22.93 Hz, 1H), 2.18 (m, 1H), 2.00 (m, 3H). ^{31}P NMR (202 MHz, $CDCl_3$): δ 32.06 (s, 1P), 30.10 (s, 1P) *isomers*. Analysis by ESI$^+$ (expected $[M + H]^+$ = 338.32. Observed $[M + H]^+$ = 338.37).

4-Fluorophenyl *N*-Benzyl-*P*-(1-hydroxy-2-oxopiperidin-3-yl)phosphonamidate (26). A solution of **19b** (25 mg, 87.65 μmol) in neat phosphorous oxychloride (100 μL) was allowed to react with end-over-end rotation for 40 min. Reaction progress was monitored by ^{31}P NMR spectroscopy, with the appearance of a peak at approximately 32 ppm and the disappearance of a peak at approximately 18 ppm, indicating completion. Then, the crude reaction mix was diluted in chloroform (5 mL), and the reaction was washed sequentially with 1 volume of the following aqueous solutions: water, saturated $NaHCO_3$, water, brine, and water. The organic layer was dried over sodium sulfate and concentrated under reduced pressure to a pale-yellow oil and used without further purification. To a solution of monochloridate, (16 mg, 41 μmol) in anhydrous CH_2Cl_2 (5 mL) with stirring at −78 °C under argon, anhydrous diisopropyl ethylamine (5 μL, 29 μmol) was added dropwise. Separately, 4-fluorophenol (4.59 mg, 41 μmol) was dissolved in anhydrous CH_2Cl_2 (500 μL) with anhydrous diisopropyl ethylamine (1 μL, 6.2 μmol); this solution was then added dropwise to the solution containing the monochloridate, *N*-benzyl-*P*-(1-(benzyloxy)-2-oxopiperidin-3-yl)-phosphonamidic chloride. The reaction was allowed to stir at −78 °C to ambient temperature for over 2 h. The reaction was then concentrated to a translucent oil, which was then purified using a reverse-phase HPLC instrument (Agilent G1361A 1260 Infinity) using a stepwise gradient (5−90% buffer B over 10 min, 90−100% buffer B over 7 min, 100% buffer B over 8 min, 100−5% buffer B over 5 min; buffer A: dH_2O with 0.1% TFA, buffer B: MeCN + 0.1% TFA). Product-containing fractions were isolated and lyophilized to a white powder, which was used without further purification. Next, a mixture of 10% palladium on carbon (20 mg) was added to THF/MeOH (2:3 ratio, 5 mL) and stirred at ambient temperature with two balloons of hydrogen for 30 min. Separately, benzylated precursor, 4-fluorophenyl *N*-benzyl-*P*-(1-(benzyloxy)-2-oxopiperidin-3-yl)-phosphonamidate (15 mg, 32 μmol) was dissolved in MeOH (500 μL) and added to the stirring suspension. The reaction was left to stir at ambient temperature for 1 h. The reaction mixture was then filtered, concentrated under reduced pressure, and purified via reverse-phase HPLC. Lyophilization yielded **26** as a white powder (12 mg, 42−47% overall). ^{1}H NMR (500 MHz, $CDCl_3$): δ 7.20 (m, 9H), 4.12 (m, 2H), 3.86 (s, 1H), 3.62 (m, 2H), 3.19 (dt, J = 23.99 Hz, 1H), 2.05 (m, 1H), 1.93 (m, 3H). ^{31}P NMR (202 MHz, $CDCl_3$) 26.46 (s, 1P), 26.26 (s, 1P) *isomers*. Analysis by ESI$^+$ (expected $[M + H]^+$ = 379.34. Observed $[M + H]^+$ = 379.38).

(((Benzylamino)(1-hydroxy-2-oxopiperidin-3-yl)-phosphoryl)oxy)methyl[1,4′-bipiperidine]-1′-carboxylate (27). Chloromethyl[1,4′-bipiperidine]-1′-carboxylate was prepared under the following conditions: to a solution of chloromethyl chloroformate (422 μL, 4.75 mmol) in CH_2Cl_2 (5 mL) was added a solution of 1,4-piperidinopiperidine (2.00 g, 11.88 mmol) in CH_2Cl_2 (5 mL) dropwise at 0 °C. A white solid precipitated out in the reaction mixture on the addition. The resulting mixture was stirred for 2 h at 0 °C and then at ambient temperature for 3 h. The reaction was monitored by thin-layer chromatography. Thereafter, the

https://doi.org/10.1021/acs.jmedchem.2c01039
J. Med. Chem. 2022, 65, 13813−13832

crude reaction was diluted with 1 volume of CH_2Cl_2 and washed twice with 1 volume of saturated $NaHCO_3$ solution and once with water. The organic layer was isolated, dried over sodium sulfate, and concentrated under reduced pressure. The resulting yellow solid (750 mg, 60.5%) was used in the next step without further purification. Next, to a solution of **19b** (60 mg, 160.27 μmol) in chloroform (2 mL), triethylamine (27 μL, 192.3 μmol) was added followed by chloromethyl[1,4′-bipiperidine]-1′-carboxylate (83.6 mg, 320.5 μmol). The solution was stirred at 50 °C for 2 h. Then, the crude reaction mixture was washed with two volumes of water. The organic layer was isolated and further washed with brine and dried over Na_2SO_4, evaporated, and concentrated under reduced pressure to yield the benzylated precursor, (((benzylamino)(1-hydroxy-2-oxopiperidin-3-yl)phosphoryl)oxy)methyl[1,4′-bipiperidine]-1′-carboxylate, as a dark yellow gum, which was lyophilized for 12 h and used without further purification. Next, a mixture of 10% palladium on carbon (50 mg) was added to THF/MeOH (2:3 ratio, 5 mL) and stirred at ambient temperature with two balloons of hydrogen for 30 min. Separately, the benzylated precursor (((benzylamino)(1-(benzyloxy)-2-oxopiperidin-3-yl)phosphoryl)oxy)methyl[1,4′-bipiperidine]-1′-carboxylate (55 mg, 91.9 μmol) was dissolved in MeOH (500 μL) and added to the stirring suspension. The reaction was left to stir at ambient temperature for another 2 h. The reaction mixture was then filtered, concentrated under reduced pressure, and purified via reverse-phase HPLC. Lyophilization yielded **27** as a yellow solid (36 mg, 77%). ^{1}H NMR (300 MHz, MeOD) 7.25 (m, 5H), 5.51 (m, 2H), 4.11 (m, 3H), 3.50 (m, 2H), 3.35 (m, 2H), 3.00 (m, 1H), 2.76 (m, 4H), 1.37−2.10 (m, 14H). ^{13}C NMR (75 MHz, MeOD): δ 162.42, 153.25, 128.21, 128.16, 127.17, 126.83, 83.37, 51.05, 49.85, 44.05, 43.76, 43.57, 42.34, 29.37, 25.97, 23.08, 26.84, 21.59. ^{31}P NMR (121 MHz, MeOD): δ 31.14 (s, 1P), 30.99 (s, 1P) *isomers*. Analysis by ESI$^+$ (expected $[M + H]^+$ = 509.56. Observed $[M + H]^+$ = 509.12).

3-(Hexadecyloxy)propyl(1-hydroxy-2-oxopiperidin-3-yl)-phosphonate (28). To a solution of 7 (5.00 g, 16.9 mmol) in pyridine (50 mL), 3-(hexadecyloxy)propan-1-ol (6.58 g, 21.9 mmol), *N*,*N*′-dicyclohexylcarbodiimide (3.68 g, 17.8 mmol), and 4-dimethylaminopyridine (207 mg, 1.70 mmol) were added. The reaction was allowed to proceed with stirring at 100 °C for 12 h. Reaction progress was monitored by ^{31}P NMR and ^{1}H−^{31}P HSQC spectroscopy and was determined to be complete upon the formation of a peak at approximately 18 ppm. The crude product was concentrated under reduced pressure at 70 °C. The residue was then diluted with CH_2Cl_2 (200 mL), washed with saturated $NaHCO_3$ (50 mL), and filtered to remove the white solid. The organic layer was isolated, dried over sodium sulfate, and concentrated under reduced pressure. The residue was diluted with EtOH (50 mL) and filtered. The filtrate was concentrated under vacuum. The residue was purified via preperatory HPLC (Phenomenex Synergi Max-RP 250 * 50 mm * 10 μm; mobile phase: water [10 mM NH_4HCO_3]−MeCN; B %: 55 MeCN %−85 MeCN %, 20 min) to give the benzylated precursor, 3-(hexadecyloxy)propyl (1-(benzyloxy)-2-oxopiperidin-3-yl)-phosphonate, as a yellow oil. The benzylated precursor, 3-(hexadecyloxy)propyl (1-(benzyloxy)-2-oxopiperidin-3-yl)-phosphonate (1.70 g, 2.99 mmol), was then dissolved in MeOH (34 mL), and 10% palladium on carbon (425 mg) was added under N_2. The suspension was degassed and purged with H_2 four times. The mixture was stirred under H_2 (15 psi) at 25 °C for 3 h, and the reaction was monitored by UPLC−MS. The crude product was filtered through a layer of diatomite and concentrated under vacuum to give a residue. The residue was dissolved in MeOH/H_2O (1/20, 63.0 mL) and lyophilized to give **28** as an off-white waxy solid (1.13 g, 36% yield). ^{1}H NMR (500 MHz, $CDCl_3$): δ 3.85 (dt, *J* = 27.31 Hz, *J* = 5.79 Hz, 2H), 3.59 (m, 2H), 3.42 (t, *J* = 6.09 Hz, 2H), 3.31 (t, *J* = 6.72 Hz, 2H), 2.85 (dt, *J* = 24.49 Hz, *J* = 6.25 Hz, 1H) 2.11 (m, 1H), 1.83−2.02 (m, 3H), 1.79 (q, *J* = 6.36 Hz, 2H), 1.47 (q, *J* = 7.70 Hz, 2H), 1.11−1.27 (m, 26H), 0.81 (t, *J* = 6.21 Hz, 3H). ^{13}C NMR (125 MHz, $CDCl_3$): δ 165.56 (s, 1C), 71.16 (s, 1C), 67.25 (s, 1C), 61.89 (s, 1C), 51.83 (s, 1C), 42.42 (d, *J* = 123.85 Hz, 1C), 31.89 (s, 1C), 31.15 (d, *J* = 4.04 Hz, 1C), 29.78 (s, 1C), 29.74 (s, 9C), 29.61 (s, 1C), 29.38 (s, 1C) 23.11 (s, 1C), 22.7 (s, 1C) 21.97 (d, *J* = 5.65 Hz, 1C), 14.05 (s, 1C). ^{31}P NMR (202 MHz, $CDCl_3$): δ 18.02 (s, 1P). Analysis by ESI$^+$ (expected $[M + H]^+$ = 478.6. Observed $[M + H]^+$ = 478.4).

Bis(cyanomethyl)(1-hydroxy-2-oxopiperidin-3-yl)-phosphonate (29). To a solution of 7 (100 mg, 351.8 μmol) in neat thionyl chloride (5 mL), a catalytic amount of DMF was added. The reaction was allowed to stir for 1 h and was monitored by ^{31}P NMR spectroscopy. Then, the reaction was diluted with 2 volumes of anhydrous CH_2Cl_2 and concentrated under reduced pressure to a dark orange oil. The crude intermediate was then dissolved immediately in anhydrous CH_2Cl_2 and cooled to −78 °C with stirring under argon. Next, a solution containing 2-cyanoethanol (200 μL, 2.9 mmol) and anhydrous triethylamine (50 μL, 358.7 μmol) in anhydrous CH_2Cl_2 was added dropwise, and the reaction was allowed to proceed for 12 h from −78 °C to ambient temperature. Reaction progress was monitored by UPLC-MS and ^{31}P NMR spectroscopy and was determined to be complete upon the disappearance of the peak at 44 pm and the appearance of a peak at 25 ppm. Thereafter, the reaction was washed sequentially with 1 volume of the following: water, saturated $NaHCO_3$, and brine. The organic layer was isolated and dried over sodium sulfate and concentrated under reduced pressure to a clear oil. Then, the benzylated precursor, bis(2-cyanoethyl)(1-(benzyloxy)-2-oxopiperidin-3-yl)phosphonate (50 mg, 127.8 μmol), was dissolved in THF/MeOH (2:3 ratio, 2 mL). Separately, a suspension of 10% palladium on carbon (50 mg) in THF/MeOH (2:3 ratio, 5 mL) was preincubated with two balloons of hydrogen for 30 min with stirring. Thereafter, the solution containing bis(2-cyanoethyl)(1-(benzyloxy)-2-oxopiperidin-3-yl)phosphonate was added to the mixture and allowed to react for 30 min. Reaction progress was monitored by $FeCl_3$ staining on thin-layer chromatography and by UPLC−MS. Upon completion, the crude compound was filtered and concentrated under reduced pressure to a clear oil. This was then purified via reverse-phase HPLC and lyophilized to a clear oil (33.9 mg, 88% yield). ^{1}H NMR (500 MHz, $CDCl_3$): δ 4.53 (m, 4H), 3.69 (q, *J* = 4.48, 4.83, 4.21 Hz, 2H), 3.26 (dt, *J* = 26.32 Hz, 1H), 2.26 (m, 3H), 1.98 (m, 1H). ^{31}P NMR (202 MHz, $CDCl_3$): δ 25.37 (s, 1P). Analysis by ESI$^+$ (expected $[M + H]^+$ = 302.24. Observed $[M + H]^+$ = 302.30).

3-(2-Oxido-4*H*-benzo[*d*][1,3,2]dioxaphosphinin-2-yl)-2-oxopiperidin-1-yl Isobutyrate (30). To a solution of **5** (500 mg, 2.56 mmol) in neat isobutyric anhydride (3 mL), triethylamine (100 μL, 717.4 μmol) was added. The solution was allowed to rotate for 15 h. Reaction progress was monitored by $FeCl_3$ staining on thin-layer chromatography and UPLC−MS. The crude product was then lyophilized for 24 h to give crude **9** as a dark orange oil, which was used without further purification. Analysis was conducted by ESI$^+$ (expected $[M + H]^+$ = 266.20; observed $[M + H]^+$ = 266.10). Next, **9** was dissolved in neat thionyl chloride (2 mL) with catalytic DMF, and the reaction was allowed to proceed for 12 h. The reaction was monitored by ^{31}P NMR spectroscopy with full conversion indicated by the emergence of the peak at 42 ppm. The reaction was then diluted with 1 volume of CH_2Cl_2 and concentrated under reduced pressure to a dark orange oil, which was used immediately without purification. The dichloride (53 mg, 194.8 μmol) was then redissolved in anhydrous CH_2Cl_2 (3.5 mL), and the solution was cooled to −78 °C under argon with stirring. Separately, 2-(hydroxymethyl)phenol (48.4 mg, 389.6 μmol) was dissolved in anhydrous CH_2Cl_2 (500 μL) with the addition of anhydrous diisopropylethylamine (5 μL, 28.7 μmol); this solution was then added dropwise to the cooled solution containing the dichloride, and the reaction was allowed to proceed for 3 h from −78 °C to ambient temperature. Reaction progress was monitored by ^{31}P NMR and ^{1}H−^{31}P HSQC spectroscopy and was determined to be complete by the presence of two peaks at 17 ppm, indicating isomers at phosphorous, and the disappearance of the peak at 42 ppm. The reaction was then quenched and washed 3 times with 1 volume of water. The organic layer containing **30** was then isolated, dried over sodium sulfate, and concentrated under reduced pressure. The product was then purified via reverse-phase HPLC and lyophilized to afford **30** as a white solid (25−41 mg, 39−65%

https://doi.org/10.1021/acs.jmedchem.2c01039
J. Med. Chem. 2022, 65, 13813−13832

yield). ^{1}H NMR (500 MHz, $CDCl_3$): δ 7.30 (t, J = 7.21, 7.78 Hz, 1H), 7.11 (m, 3H), 5.42 (d, J = 14.33 Hz, 1H), 5.37 (d, J = 12.95 Hz, 1H), 3.70 (m, 1H), 3.62 (m, 1H), 3.38 (dt, J = 25.36 Hz, 1H), 2.67 (m, 1H), 2.36 (m, 2H), 2.27 (m, 1H), 2.02 (m, 1H), 1.19 (m, 6H). ^{31}P NMR (202 MHz, $CDCl_3$): δ 17.70 (s, 1P), 17.14 (s, 1P) *isomers*. Analysis by ESI$^+$ (expected $[M + H]^+$ = 354.31. Observed $[M + H]^+$ = 354.17).

Enolase Activity Assay and Inhibitor Titrations. See ref 71 for assay methods. Reactions were performed with 5 mM 2-PG. Data presented are the mean ± SD of $N \geq 5$.

Cell Lines for Activity Screenings. Cell culture experiments were performed using the following cell lines: D423-MG, D423 *ENO1*, LN319, and, in some cases, Gli56. The D423-MG cell line is 1p36 homozygously deleted from *CAMTA1* to *SLC25A33*, which includes *ENO1*. D423 *ENO1* is an isogenic ectopically rescued cell line that was described previously (pCMV *ENO1* 5X).[5] LN319 is an *ENO1*-WT cell line used as a control for sensitivity to enolase inhibitor prodrugs. In some experiments, the *ENO1*-homozygous deleted cell line Gli56 was also used and was characterized previously.[8] Cells were regularly cultured in Dulbecco's modified Eagle's medium (DMEM) supplemented with 10% fetal bovine serum.

In Vitro Cytotoxicity of Prodrugs. Cell culture experiments performed in the three-cell line assay were conducted in 96-well plates. Plates were seeded at approximately 15% confluence (10^3 cells per well). Cancer cells were attached for 24 h and were treated with fresh medium containing a prodrug inhibitor. Columns 1−2 and 11−12 were used as vehicle-medium-only control wells. Columns 3−10 were used for drug treatment in twofold concentration gradients. Treatment with the enolase inhibitor prodrug proceeded for 6 days unless otherwise noted. Thereafter, the plates were washed with PBS and fixed with 10% formalin. The fixed plates were stained with 0.1% crystal violet and quantified by acetic acid extraction with spectrophotometric absorption at 595 nm in a plate reader.[72,73] Cell densities were expressed relative to non-drug, medium-only wells. All experiments were conducted in DMEM with 4.5 g/L glucose, 110 mg/L pyruvate, and 584 mg/L glutamine (Cellgro/Corning no. 10-013-CV) with 10% FBS (Gibco/Life Technologies no. 16140−071), 1% penicillin−streptomycin (Gibco/Life Technologies no. 15140−122), and 0.1% amphotericin B (Gibco/Life Technologies no. 15290-018).

NCI-60 Cell Line Screening. Compound screening in the NCI-60 cell line panel is a service provided by the Developmental Therapeutics Program in the Division of Cancer Treatment and Diagnosis at the NCI. All compounds were tested at a single 10 μM dose across 60 cell lines for 24 h. Certain cell lines were not included in some experiments due to unavailability, as indicated in Figures 3 and S4−S6. One-dose inhibitory data are reported relative to a drug-free, untreated control and are relative to the number of cells present at time zero. All cell lines are grown in RPMI 1640 medium containing 5% FBS and 2 mM L-glutamine. Experiments were conducted in 96-well plates. The plates were seeded at densities ranging from 5000 to 40,000 cells/well depending on the doubling time of individual cell lines. Full experimental conditions are available on the NCI-60 screening methodology: https://dtp.cancer.gov/discovery_development/nci-60/methodology.htm.

Prodrug Stability Assay. The stability of the prodrugs was assessed by time-course ^{31}P NMR spectroscopy at prespecified timepoints using a Bruker AVANCE HD III 500 MHz or 300 MHz. Compounds were dissolved in DMSO and added to a solution containing either 80% human serum supplemented with 20% D_2O or 80% DMEM supplemented with 20% D_2O. Final prodrug concentrations were 2 mM, unless otherwise indicated. Scans were obtained on using the ^{31}P CPD pulse sequence (ns = 500). Where applicable, two-dimensional ^{1}H−^{31}P HSQC spectra were obtained by changing F_2 to ^{31}P on the HSQCETGP pulse sequence used for the ^{1}H−^{13}C HSQC pulse sequence and then by entering the following parameters: ns = 10, gpz2 = 32.4, sw = 40, o2p = 0, cnst2 = 22.95 (specifically adjusted to view the $^2J_{P-H}$ coupling on **5**), followed by the "getprosal" command.[51] Between timepoints, samples were incubated at 37 °C to better emulate physiological conditions. Spectra were processed using MestReNova Version 14.1.1, and peak integrations for prodrugs and metabolites are expressed relative to the phosphate peak in the serum at 0 ppm.

■ ASSOCIATED CONTENT

Supporting Information

The Supporting Information is available free of charge at https://pubs.acs.org/doi/10.1021/acs.jmedchem.2c01039.

Dose response curves for prodrugs, plasma stability of select prodrugs, activity in the NCI-60 cell line panel for select prodrugs, and NMR spectra for the final compounds (PDF)

Molecular formula strings (CSV)

Raw data from the NCI-60 cell line screening panel for select prodrugs (XLSX)

■ AUTHOR INFORMATION

Corresponding Author

Victoria C. Yan − *Department of Cancer Systems Imaging, University of Texas MD Anderson Cancer Center, Houston, Texas 77054, United States;* orcid.org/0000-0003-0837-5184; Email: victoriacyanide@gmail.com; @victoriacyanide

Authors

Cong-Dat Pham − *Department of Cancer Systems Imaging, University of Texas MD Anderson Cancer Center, Houston, Texas 77054, United States*

Elliot S. Ballato − *Department of Cancer Systems Imaging, University of Texas MD Anderson Cancer Center, Houston, Texas 77054, United States*

Kristine L. Yang − *Department of Cancer Systems Imaging, University of Texas MD Anderson Cancer Center, Houston, Texas 77054, United States*

Kenisha Arthur − *Department of Cancer Systems Imaging, University of Texas MD Anderson Cancer Center, Houston, Texas 77054, United States*

Sunada Khadka − *Department of Cancer Systems Imaging, University of Texas MD Anderson Cancer Center, Houston, Texas 77054, United States; Department of Cancer Biology, University of Texas MD Anderson Cancer Center, Houston, Texas 77054, United States*

Yasaman Barekatain − *Department of Cancer Systems Imaging, University of Texas MD Anderson Cancer Center, Houston, Texas 77054, United States; Department of Cancer Biology, University of Texas MD Anderson Cancer Center, Houston, Texas 77054, United States;* orcid.org/0000-0002-4454-1496

Prakriti Shrestha − *Department of Cancer Systems Imaging, University of Texas MD Anderson Cancer Center, Houston, Texas 77054, United States*

Theresa Tran − *Department of Cancer Systems Imaging, University of Texas MD Anderson Cancer Center, Houston, Texas 77054, United States*

Anton H. Poral − *Department of Cancer Systems Imaging, University of Texas MD Anderson Cancer Center, Houston, Texas 77054, United States*

Mykia Washington − *Department of Cancer Systems Imaging, University of Texas MD Anderson Cancer Center, Houston, Texas 77054, United States*

Sudhir Raghavan − *Department of Cancer Systems Imaging, University of Texas MD Anderson Cancer Center, Houston, Texas 77054, United States*
Barbara Czako − *Institute of Applied Cancer Science, University of Texas MD Anderson Cancer Center, Houston, Texas 77054, United States*
Federica Pisaneschi − *Department of Cancer Systems Imaging, University of Texas MD Anderson Cancer Center, Houston, Texas 77054, United States*
Yu-Hsi Lin − *Department of Cancer Systems Imaging, University of Texas MD Anderson Cancer Center, Houston, Texas 77054, United States;* orcid.org/0000-0001-5763-1530
Nikunj Satani − *Department of Cancer Systems Imaging, University of Texas MD Anderson Cancer Center, Houston, Texas 77054, United States;* orcid.org/0000-0003-3908-3731
Naima Hammoudi − *Department of Cancer Systems Imaging, University of Texas MD Anderson Cancer Center, Houston, Texas 77054, United States*
Jeffrey J. Ackroyd − *Department of Cancer Systems Imaging, University of Texas MD Anderson Cancer Center, Houston, Texas 77054, United States*
Dimitra K. Georgiou − *Department of Cancer Systems Imaging, University of Texas MD Anderson Cancer Center, Houston, Texas 77054, United States*
Steven W. Millward − *Department of Cancer Systems Imaging, University of Texas MD Anderson Cancer Center, Houston, Texas 77054, United States;* orcid.org/0000-0002-3231-7075
Florian L. Muller − *Department of Cancer Systems Imaging, University of Texas MD Anderson Cancer Center, Houston, Texas 77054, United States;* orcid.org/0000-0001-7568-2948

Complete contact information is available at: https://pubs.acs.org/10.1021/acs.jmedchem.2c01039

Author Contributions

V.C.Y., C.-D.P., E.S.B., K.L.Y., S.R., B.C., and F.P. synthesized and characterized compounds. K.A., S.K., P.S., T.T., A.H.P., M.W., N.H., J.J.A., and D.K.G. performed cell culture experiments. N.S. performed enzyme activity assays. V.C.Y., Y.-H.L., C.-D.P., Y.B., and E.S.B. performed NMR assays. S.W.M. and F.L.M. provided critical comments and suggestions. V.C.Y. and F.L.M. designed experiments and oversaw this work. V.C.Y. analyzed data and wrote the manuscript. All authors have given approval to the final version of this manuscript.

Notes

The authors declare the following competing financial interest(s): F.L.M., V.C.Y., E.S.B., K.L.Y., and C-D.P., are inventors on a patent describing compounds included in this work (WO/2020/154742). V.C.Y., C-D.P., and F.L.M. are inventors on a patent describing methods of preparation for compounds included in this work (US 63/004,063). F.L.M., F.P., B.C., Y-H.L., and N.S., are inventors on a patent describing the concept of targeting *ENO1*-deleted cancers with inhibitors of ENO2 (US 10,363,261). F.L.M. is an inventor on a separate patent describing the concept of targeting *ENO1*-deleted tumors with inhibitors of ENO2 (US 9,452,182 B2).

ACKNOWLEDGMENTS

We thank Kumar Kalurachchi for assistance with NMR studies and the NCI Developmental Therapeutics Program for conducing the NCI-60 cell line screens. The MD Anderson Cancer Center NMR Core Facility is supported in part by the NCI Cancer Center Support Grant (CA16672). S.K. is supported by the Larry Deaven Fellowship and a CPRIT research training grant (RP170067). Y.B. is supported by a CPRIT research training grant (RP210028), the Dr. John J. Kopchick Fellowship, and the Schissler Foundation. This work was funded by research grants from the American Cancer Society (RSG-15-145-01-CDD; F.L.M.), National Comprehensive Cancer Network (YIA170032; F.L.M.), Andrew Sabin Family Foundation (F.L.M.), Dr. Marnie Rose Foundation (F.L.M.), Uncle Kory Foundation (F.L.M.), University of Texas MD Anderson Cancer Center Institutional Research grant (F.L.M.), and the NIH (R01 CA231509-01A1; S.W.M.).

ABBREVIATIONS

2-PG, 2-phosphoglycerate; BOM, benzoyloxymethyl; CNS, central nervous system; CPD, composite pulse decoupling; *ENO1*, enolase 1; ENO2, enolase 2; FBS, fetal bovine serum; GBM, glioblastoma; HINT1, histidine nucleotide triad-binding protein 1; IC_{50}, half-maximal inhibitory concentration; IP, intraperitoneal; NCI, National Cancer Institute; NSCLC, non-small-cell lung cancer; PDB, Protein Data Bank; PEP, phosphoenolpyruvate; POC, isopropyloxymethyl carbonate; POM, pivaloyloxymethyl; PhAH, phosphoacetohydroxamate; SATE, *S*-acyl-2-thioethyl; TAF, tenofovir alafenamide

REFERENCES

(1) Vander Heiden, M. G.; Cantley, L. C.; Thompson, C. B. Understanding the Warburg Effect: The Metabolic Requirements of Cell Proliferation. *Science* **2009**, *324*, 1029−1033.
(2) Hay, N. Reprogramming Glucose Metabolism in Cancer: Can It Be Exploited for Cancer Therapy? *Nat. Rev. Cancer* **2016**, *16*, 635−649.
(3) Warburg, O. On the Origin of Cancer Cells. *Science* **1956**, *123*, 309−314.
(4) Stine, Z. E.; Schug, Z. T.; Salvino, J. M.; Dang, C. V. Targeting Cancer Metabolism in the Era of Precision Oncology. *Nat. Rev. Drug Discovery* **2022**, *21*, 141−162.
(5) Muller, F. L.; Colla, S.; Aquilanti, E.; Manzo, V. E.; Genovese, G.; Lee, J.; Eisenson, D.; Narurkar, R.; Deng, P.; Nezi, L.; Lee, M. A.; Hu, B.; Hu, J.; Sahin, E.; Ong, D.; Fletcher-Sananikone, E.; Ho, D.; Kwong, L.; Brennan, C.; Wang, Y. A.; Chin, L.; DePinho, R. A. Passenger Deletions Generate Therapeutic Vulnerabilities in Cancer. *Nature* **2012**, *488*, 337−342.
(6) Muller, F. L.; Aquilanti, E. A.; DePinho, R. A. Collateral Lethality: A New Therapeutic Strategy in Oncology. *Trends Cancer* **2015**, *1*, 161−173.
(7) Schwartzbaum, J. A.; Fisher, J. L.; Aldape, K. D.; Wrensch, M. Epidemiology and Molecular Pathology of Glioma. *Nat. Clin. Pract. Neurol.* **2006**, *2*, 494−503.
(8) Leonard, P. G.; Satani, N.; Maxwell, D.; Lin, Y.-H.; Hammoudi, N.; Peng, Z.; Pisaneschi, F.; Link, T. M.; Lee, G. R.; Sun, D.; Prasad, B. A. B.; Di Francesco, M. E.; Czako, B.; Asara, J. M.; Wang, Y. A.; Bornmann, W.; DePinho, R. A.; Muller, F. L. SF2312 Is a Natural Phosphonate Inhibitor of Enolase. *Nat. Chem. Biol.* **2016**, *12*, 1053−1058.
(9) Anderson, V. E.; Weiss, P. M.; Cleland, W. W. Reaction intermediate analogs for enolase. *Biochemistry* **1984**, *23*, 2779−2786.
(10) Kang, H. J.; Jung, S. K.; Kim, S. J.; Chung, S. J. Structure of human α-enolase (hENO1), a multifunctional glycolytic enzyme. *Acta Crystallogr., Sect. D: Biol. Crystallogr.* **2008**, *64*, 651−657.

(11) Qin, J.; Chai, G.; Brewer, J. M.; Lovelace, L. L.; Lebioda, L. Structures of Asymmetric Complexes of Human Neuron Specific Enolase with Resolved Substrate and Product and an Analogous Complex with Two Inhibitors Indicate Subunit Interaction and Inhibitor Cooperativity. *J. Inorg. Biochem.* **2012**, *111*, 187−194.
(12) Lin, Y. H.; Satani, N.; Hammoudi, N.; Yan, V. C.; Barekatain, Y.; Khadka, S.; Ackroyd, J. J.; Georgiou, D. K.; Pham, C. D.; Arthur, K.; Maxwell, D.; Peng, Z.; Leonard, P. G.; Czako, B.; Pisaneschi, F.; Mandal, P.; Sun, Y.; Zielinski, R.; Pando, S. C.; Wang, X.; Tran, T.; Xu, Q.; Wu, Q.; Jiang, Y.; Kang, Z.; Asara, J. M.; Priebe, W.; Bornmann, W.; Marszalek, J. R.; DePinho, R. A.; Muller, F. L. An Enolase Inhibitor for the Targeted Treatment of ENO1-Deleted Cancers. *Nat. Metab.* **2020**, *2*, 1413−1426.
(13) Jezewski, A. J.; Lin, Y.-H.; Reisz, J. A.; Culp-Hill, R.; Barekatain, Y.; Yan, V. C.; D'Alessandro, A.; Muller, F. L.; Odom John, A. R. Targeting Host Glycolysis as a Strategy for Antimalarial Development. *Front. Cell. Infect. Microbiol.* **2021**, *11*, 730413.
(14) Pisaneschi, F.; Lin, Y. H.; Leonard, P. G.; Satani, N.; Yan, V. C.; Hammoudi, N.; Raghavan, S.; Link, T. M.; Georgiou, D. K.; Czako, B.; Muller, F. L. The 3S Enantiomer Drives Enolase Inhibitory Activity in SF2312 and Its Analogues. *Molecules* **2019**, *24*, 2510.
(15) Starrett, J. E.; Tortolani, D. R.; Russell, J.; Hitchcock, M. J. M.; Whiterock, V.; Martin, J. C.; Mansuri, M. M. Synthesis, Oral Bioavailability Determination, and in Vitro Evaluation of Prodrugs of the Antiviral Agent 9-[2-(Phosphonomethoxy)Ethyl]Adenine (PMEA). *J. Med. Chem.* **1994**, *37*, 1857−1864.
(16) Arimilli, M. N.; Kim, C. U.; Dougherty, J.; Mulato, A.; Oliyai, R.; Shaw, J. P.; Cundy, K. C.; Bischofberger, N. Synthesis, in Vitro Biological Evaluation and Oral Bioavailability of 9-[2-(Phosphonomethoxy)Propyl]Adenine (PMPA) Prodrugs. *Antiviral Chem. Chemother.* **1997**, *8*, 557−564.
(17) Eisenberg, E. J.; He, G.-X.; Lee, W. A. Metabolism of GS-7340, A Novel Phenyl Monophosphoramidate Intracellular Prodrug of PMPA, in Blood. *Nucleosides, Nucleotides Nucleic Acids* **2001**, *20*, 1091−1098.
(18) Farquhar, D.; Srivastva, D. N.; Kuttesch, N. J.; Saunders, P. P. Biologically Reversible Phosphate-Protective Groups. *J. Pharm. Sci.* **1983**, *72*, 324−325.
(19) Srivastva, D. N.; Farquhar, D. Bioreversible Phosphate Protective Groups: Synthesis and Stability of Model Acyloxymethyl Phosphates. *Bioorg. Chem.* **1984**, *12*, 118−129.
(20) Farquhar, D.; Khan, S.; Srivastva, D. N.; Saunders, P. P. Synthesis and Antitumor Evaluation of Bis[(pivaloyloxy)methyl] 2′-Deoxy-5-fluorouridine 5′ -Monophosphate (FdUMP): A Strategy To Introduce Nucleotides into Cells. *J. Med. Chem.* **1994**, *37*, 3902−3909.
(21) Khadka, S.; Arthur, K.; Barekatain, Y.; Behr, E.; Washington, M.; Ackroyd, J.; Crowley, K.; Suriyamongkol, P.; Lin, Y.; Pham, C.; Zielinski, R.; Trujillo, M.; Galligan, J.; Georgiou, D. K.; Asara, J.; Muller, F. Impaired Anaplerosis Is a Major Contributor to Glycolysis Inhibitor Toxicity in Glioma. *Cancer Metabol.* **2021**, *9*, 27.
(22) McGuigan, C.; Pathirana, R. N.; Mahmood, N.; Hay, A. J. Aryl Phosphate Derivates of AZT Inhibit HIV Replication in Cells Where the Nucleoside Is Poorly Active. *Bioorg. Med. Chem. Lett.* **1992**, *2*, 701−704.
(23) Erion, M. D.; Reddy, K. R.; Boyer, S. H.; Matelich, M. C.; Gomez-Galeno, J.; Lemus, R. H.; Ugarkar, B. G.; Colby, T. J.; Schanzer, J.; van Poelje, P. D. Design, Synthesis, and Characterization of a Series of Cytochrome P450 3A-Activated Prodrugs (HepDirect Prodrugs) Useful for Targeting Phosph(on)ate-Based Drugs to the Liver. *J. Am. Chem. Soc.* **2004**, *126*, 5154−5163.
(24) Alanazi, A. S.; Miccoli, A.; Mehellou, Y. Aryloxy Pivaloyloxymethyl Prodrugs as Nucleoside Monophosphate Prodrugs. *J. Med. Chem.* **2021**, *64*, 16703−16710.
(25) Pradere, U.; Garnier-Amblard, E. C.; Coats, S. J.; Amblard, F.; Schinazi, R. F. Synthesis of Nucleoside Phosphate and Phosphonate Prodrugs. *Chem. Rev.* **2014**, *114*, 9154−9218.
(26) Mikati, M.; Miller, J.; Osbourn, D.; Barekatain, Y.; Ghebremichael, N.; Shah, I.; Burnham, C.-A. D.; Heidel, K.; Yan, V.; Muller, F.; Dowd, C.; Edwards, R.; Odom John, A. Antimicrobial Prodrug Activation by the Staphylococcal Glyoxalase GloB. *ACS Infect. Dis.* **2020**, *6*, 3064−3075.
(27) Reiser, H.; Wang, J.; Chong, L.; Watkins, W. J.; Ray, A. S.; Shibata, R.; Birkus, G.; Cihlar, T.; Wu, S.; Li, B.; Liu, X.; Henne, L. N.; Wolfgang, G. H. I.; Desai, M.; Rhodes, G. R.; Fridland, A.; Lee, W. A.; Plunkett, W.; Vail, D.; Thamm, D. H.; Jeraj, R.; Tumas, D. B. GS-9219-A Novel Acyclic Nucleotide Analogue with Potent Antineoplastic Activity in Dogs with Spontaneous Non-Hodgkin's Lymphoma. *Clin. Cancer Res.* **2008**, *14*, 2824−2832.
(28) Cihlar, T.; Ray, A. S.; Boojamra, C. G.; Zhang, L.; Hui, H.; Laflamme, G.; Vela, J. E.; Grant, D.; Chen, J.; Myrick, F.; White, K. L.; Gao, Y.; Lin, K. Y.; Douglas, J. L.; Parkin, N. T.; Carey, A.; Pakdaman, R.; Mackman, R. L. Design and Profiling of GS-9148, a Novel Nucleotide Analog Active against Nucleoside-Resistant Variants of Human Immunodeficiency Virus Type 1, and Its Orally Bioavailable Phosphonoamidate Prodrug, GS-9131. *Antimicrob. Agents Chemother.* **2008**, *52*, 655−665.
(29) Lee, W. A.; He, G.-X.; Eisenberg, E.; Cihlar, T.; Swaminathan, S.; Mulato, A.; Cundy, K. C. Selective Intracellular Activation of a Novel Prodrug of the Human Immunodeficiency Virus Reverse Transcriptase Inhibitor Tenofovir Leads to Preferential Distribution and Accumulation in Lymphatic Tissue. *Antimicrob. Agents Chemother.* **2005**, *49*, 1898−1906.
(30) Dang, Q.; Liu, Y.; Cashion, D. K.; Kasibhatla, S. R.; Jiang, T.; Taplin, F.; Jacintho, J. D.; Li, H.; Sun, Z.; Fan, Y.; DaRe, J.; Tian, F.; Li, W.; Gibson, T.; Lemus, R.; van Poelje, P. D.; Potter, S. C.; Erion, M. D. Discovery of a Series of Phosphonic Acid-Containing Thiazoles and Orally Bioavailable Diamide Prodrugs That Lower Glucose in Diabetic Animals through Inhibition of Fructose-1,6-Bisphosphatase. *J. Med. Chem.* **2011**, *54*, 153−165.
(31) Murakami, E.; Tolstykh, T.; Bao, H.; Niu, C.; Steuer, H. M.; Bao, D.; Chang, W.; Espiritu, C.; Bansal, S.; Lam, A. M.; Otto, M. J.; Sofia, M. J.; Furman, P. A. Mechanism of Activation of PSI-7851 and Its Diastereoisomer PSI-7977. *J. Biol. Chem.* **2010**, *285*, 34337−34347.
(32) Yan, V. C.; Pham, C. D.; Arthur, K.; Yang, K. L.; Muller, F. L. Aliphatic Amines Are Viable Pro-Drug Moieties in Phosphonoamidate Drugs. *Bioorg. Med. Chem. Lett.* **2020**, *30*, 127656.
(33) Murakami, E.; Wang, T.; Babusis, D.; Lepist, E.-I.; Sauer, D.; Park, Y.; Vela, J. E.; Shih, R.; Birkus, G.; Stefanidis, D.; Kim, C. U.; Cho, A.; Ray, A. S. Metabolism and Pharmacokinetics of the Anti-Hepatitis C Virus Nucleotide Prodrug GS-6620. *Antimicrob. Agents Chemother.* **2014**, *58*, 1943−1951.
(34) Li, R.; Liclican, A.; Xu, Y.; Pitts, J.; Niu, C.; Zhang, J.; Kim, C.; Zhao, X.; Soohoo, D.; Babusis, D.; Yue, Q.; Ma, B.; Murray, B. P.; Subramanian, R.; Xie, X.; Zou, J.; Bilello, J. P.; Li, L.; Schultz, B. E.; Sakowicz, R.; Smith, B. J.; Shi, P.-Y.; Murakami, E.; Feng, J. Y. Key Metabolic Enzymes Involved in Remdesivir Activation in Human Lung Cells. *Antimicrob. Agents Chemother.* **2021**, *65*, No. e0060221.
(35) Birkus, G.; Kutty, N.; Frey, C. R.; Shribata, R.; Chou, T.; Wagner, C.; McDermott, M.; Cihlar, T. Role of Cathepsin A and Lysosomes in the Intracellular Activation of Novel Antipapillomavirus Agent GS-9191. *Antimicrob. Agents Chemother.* **2011**, *55*, 2166−2173.
(36) Birkus, G.; Kutty, N.; He, G.; Mulato, A.; Lee, W.; McDermott, M.; Cihlar, T. Activation of 9-[(R)-2-[[(S)-[[(S)-1-(Isopropoxycarbonyl)ethyl]amino] phenoxyphosphinyl]-methoxy]-propyl]adenine (GS-7340) and Other Tenofovir Phosphonoamidate Prodrugs by Human Proteases. *Mol. Pharmacol.* **2008**, *74*, 92−100.
(37) Birkus, G.; Wang, R.; Liu, X.; Kutty, N.; MacArthur, H.; Cihlar, T.; Gibbs, C.; Swaminathan, S.; Lee, W.; McDermott, M. Cathepsin A Is the Major Hydrolase Catalyzing the Intracellular Hydrolysis of the Antiretroviral Nucleotide Phosphonoamidate Prodrugs GS-7340 and GS-9131. *Antimicrob. Agents Chemother.* **2007**, *51*, 543−550.
(38) Lentini, N. A.; Foust, B. J.; Hsiao, C. H. C.; Wiemer, A. J.; Wiemer, D. F. Phosphonamidate Prodrugs of a Butyrophilin Ligand Display Plasma Stability and Potent Vγ9 Vδ2 T Cell Stimulation. *J. Med. Chem.* **2018**, *61*, 8658−8669.

(39) Kadri, H.; Taher, T. E.; Xu, Q.; Sharif, M.; Ashby, E.; Bryan, R. T.; Willcox, B. E.; Mehellou, Y. Aryloxy Diester Phosphonamidate Prodrugs of Phosphoantigens (ProPAgens) as Potent Activators of Vγ9/Vδ2 T-Cell Immune Responses. *J. Med. Chem.* **2020**, *63*, 11258−11270.
(40) Sizun, G.; Pierra, C.; Badaroux, E.; Rabeson, C.; Benzaria-Prad, S.; Surleraux, D.; Loi, A. G.; Musiu, C.; Liuzzu, M.; Seifer, M.; Standring, D.; Sommadossi, J.-P.; Gosselin, G. Design, Synthesis and Antiviral Evaluation of 2′-C-Methyl Branched Guanosine Pronucleotides: The Discovery of IDX184, a Potent Liver-Targeted HCV Polymerase Inhibitor. *Future Med. Chem.* **2015**, *7*, 1675.
(41) Yan, V. C.; Yang, K. L.; Ballato, E. S.; Khadka, S.; Shrestha, P.; Arthur, K.; Georgiou, D. K.; Washington, M.; Tran, T.; Poral, A. H.; Pham, C.-D.; Yan, M. J.; Muller, F. L. Bioreducible Phosphonoamidate Pro-Drug Inhibitor of Enolase: Proof of Concept Study. *ACS Med. Chem. Lett.* **2020**, *11*, 1484−1489.
(42) Letsinger, R. L.; Ogilvie, K. K. Nucleotide chemistry. XIII. Synthesis of oligothymidylates via phosphotriester intermediates. *J. Am. Chem. Soc.* **1969**, *91*, 3350−3355.
(43) Reese, C. B. The Chemical Synthesis of Oligo- and Poly-Nucleotides by the Phosphotriester Approach. *Tetrahedron* **1978**, *34*, 3143−3179.
(44) Morton, C. L.; Wadkins, R. M.; Danks, M. K.; Potter, P. M. The Anticancer Prodrug CPT-11 Is a Potent Inhibitor of Acetylcholinesterase but Is Rapidly Catalyzed to SN-38 by Butyrylcholinesterase. *Cancer Res.* **1999**, *59*, 1458−1463.
(45) Cantu, D. C.; Chen, Y.; Reilly, P. J. Thioesterases: A new perspective based on their primary and tertiary structures. *Protein Sci.* **2010**, *19*, 1281−1295.
(46) Hu, J.; Handisides, D. R.; Van Valckenborgh, E.; De Raeve, H.; Menu, E.; Vande Broek, I.; Liu, Q.; Sun, J. D.; Van Camp, B.; Hart, C. P.; Vanderkerken, K. Targeting the Multiple Myeloma Hypoxic Niche with TH-302, a Hypoxia-Activated Prodrug. *Blood* **2010**, *116*, 1524−1527.
(47) Lespinasse, F.; Thomas, C.; Bonnay, M.; Malaise, E. P.; Guichard, M. Ro 03-8799: Preferential relative uptake in human tumor xenografts compared to a murine tumor: Comparison with SR-2508. *Int. J. Radiat. Oncol., Biol., Phys.* **1989**, *16*, 1105−1109.
(48) Gammon, S. T.; Pisaneschi, F.; Bandi, M. L.; Smith, M. G.; Sun, Y.; Rao, Y.; Muller, F.; Wong, F.; De Groot, J.; Ackroyd, J.; Mawlawi, O.; Davies, M. A.; Vashisht Gopal, Y. N.; Di Francesco, M. E.; Marszalek, J. R.; Dewhirst, M.; Piwnica-Worms, D. Mechanism-Specific Pharmacodynamics of a Novel Complex-I Inhibitor Quantified by Imaging Reversal of Consumptive Hypoxia with [18F]FAZA PET In Vivo. *Cells* **2019**, *8*, 1487.
(49) Saunderes, M. I.; Dischee, S.; Fermont, D.; Bishop, A.; Lenox-Smith, I.; Allen, J. G.; Malcom, S. L. The Radiosensitizer Ro 03-8799 and the Concentrations Which May Be Achieved in Human Tumours: A Preliminary Study. *Br. J. Cancer* **1982**, *46*, 706−710.
(50) Barekatain, Y.; Yan, V. C.; Arthur, K.; Ackroyd, J. J.; Khadka, S.; De Groot, J.; Huse, J. T.; Muller, F. L. Robust Detection of Oncometabolic Aberrations by 1H−13C Heteronuclear Single Quantum Correlation in Intact Biological Specimens. *Commun. Biol.* **2020**, *3*, 328.
(51) Barekatain, Y.; Khadka, S.; Harris, K.; Delacerda, J.; Yan, V. C.; Chen, K.-C.; Pham, C.-D.; Uddin, M. N.; Avritcher, R.; Eisenberg, E. J.; Kalluri, R.; Millward, S. W.; Muller, F. L. Quantification of Phosphonate Drugs by 1H-31P HSQC Shows That Rats Are Better Models of Primate Drug Exposure than Mice. *Anal. Chem.* **2022**, *94*, 10045−10053.
(52) Buller, R. M.; Owens, G.; Schriewer, J.; Melman, L.; Beadle, J. R.; Hostetler, K. Y. Efficacy of Oral Active Ether Lipid Analogs of Cidofovir in a Lethal Mousepox Model. *Virology* **2004**, *318*, 474−481.
(53) Schooley, R. T.; Carlin, A. F.; Beadle, J. R.; Valiaeva, N.; Zhang, X. Q.; Clark, A. E.; McMillan, R. E.; Leibel, S. L.; McVicar, R. N.; Xie, J.; Garretson, A. F.; Smith, V. I.; Murphy, J.; Hostetler, K. Y. Rethinking Remdesivir: Synthesis, Antiviral Activity, and Pharmacokinetics of Oral Lipid Prodrugs. *Antimicrob. Agents Chemother.* **2021**, *65*, No. e0115521.
(54) Pribut, N.; D'Erasmo, M.; Dasari, M.; Giesler, K. E.; Iskandar, S.; Sharma, S. K.; Bartsch, P. W.; Raghuram, A.; Bushnev, A.; Hwang, S. S.; Burton, S. L.; Derdeyn, C. A.; Basson, A. E.; Liotta, D. C.; Miller, E. J. ω-Functionalized Lipid Prodrugs of HIV NtRTI Tenofovir with Enhanced Pharmacokinetic Properties. *J. Med. Chem.* **2021**, *64*, 12917−12937.
(55) Meier, C.; Görbig, U.; Müller, C.; Balzarini, J. CycloSal-PMEA and CycloAmb-PMEA: Potentially New Phosphonate Prodrugs Based on the Cyclosal-Pronucleotide Approach. *J. Med. Chem.* **2005**, *48*, 8079−8086.
(56) Matsuzawa, Y.; Hostetler, K. Y. Properties of Phospholipase C Isolated from Rat Liver Lysosomes. *J. Biol. Chem.* **1980**, *255*, 646−652.
(57) Sun, S.; Lee, D.; Lee, N. P.; Pu, J. K. S.; Wong, S. T. S.; Lui, W. M.; Fung, C. F.; Leung, G. K. K. Hyperoxia Resensitizes Chemoresistant Human Glioblastoma Cells to Temozolomide. *J. Neurooncol.* **2012**, *109*, 467−475.
(58) Stupp, R.; Mason, W. P.; van den Bent, M. J.; Weller, M.; Fisher, B.; Taphoorn, M. J.; Belanger, K.; Brandes, A. A.; Marosi, C.; Bogdahn, U.; Curschmann, J.; Janzer, R. C.; Ludwin, S. K.; Gorlia, T.; Allgeier, A.; Lacombe, D.; Cairncross, G.; Eisenhauer, E.; Mirimanoff, R. O. Radiotherapy plus Concomitant and Adjuvant Temozolomide for Glioblastoma. *N. Engl. J. Med.* **2005**, *352*, 987−996.
(59) Stupp, R.; Hegi, M. E.; Mason, W. P.; van den Bent, M. J.; Taphoorn, M. J.; Janzer, R. C.; Ludwin, S. K.; Allgeier, A.; Fisher, B.; Belanger, K.; Hau, P.; Brandes, A. A.; Gijtenbeek, J.; Marosi, C.; Vecht, C. J.; Mokhtari, K.; Wesseling, P.; Villa, S.; Eisenhauer, E.; Gorlia, T.; Weller, M.; Lacombe, D.; Cairncross, J. G.; Mirimanoff, R. O. Effects of Radiotherapy with Concomitant and Adjuvant Temozolomide versus Radiotherapy Alone on Survival in Glioblastoma in a Randomised Phase III Study: 5-Year Analysis of the EORTC-NCIC Trial. *Lancet Oncol.* **2009**, *10*, 459−466.
(60) Borch, R. F.; Liu, J.; Schmidt, J. P.; Marakovits, J. T.; Joswig, C.; Gipp, J. J.; Mulcahy, R. T. Synthesis and Evaluation of Nitroheterocyclic Phosphoramidates as Hypoxia-Selective Alkylating Agents. *J. Med. Chem.* **2000**, *43*, 2258−2265.
(61) Serpi, M.; Bibbo, R.; Rat, S.; Roberts, H.; Hughes, C.; Caterson, B.; Alcaraz, M. J.; Gibert, A. T.; Verson, C. R. A.; McGuigan, C. Novel Phosphoramidate Prodrugs of N-Acetyl-(d)-Glucosamine with Antidegenerative Activity on Bovine and Human Cartilage Explants. *J. Med. Chem.* **2012**, *55*, 4629−4639.
(62) Miccoli, A.; Dhiani, B. A.; Mehellou, Y. Phosphotyrosine Prodrugs: Design, Synthesis and Anti-STAT3 Activity of ISS-610 Aryloxy Triester Phosphoramidate Prodrugs. *Medchemcomm* **2019**, *10*, 200−208.
(63) Elbaum, D.; Beconi, M. G.; Monteagudo, E.; Di Marco, A.; Quinton, M. S.; Lyons, K. A.; Vaino, A.; Harper, S. Fosmetpantotenate (RE-024), a Phosphopantothenate Replacement Therapy for Pantothenate Kinase-Associated Neurodegeneration: Mechanism of Action and Efficacy in Nonclinical Models. *PLoS One* **2018**, *13*, No. e0192028.
(64) Imai, T.; Taketani, M.; Shii, M.; Hosokawa, M.; Chiba, K. Substrate Specificity of Carboxylesterase Isozymes and Their Contribution to Hydrolase Activity in Human Liver and Small Intestine. *Drug Metab. Dispos.* **2006**, *34*, 1734−1741.
(65) Bender, A. T.; Beavo, J. A. Cyclic Nucleotide Phosphodiesterases: Molecular Regulation to Clinical Use. *Pharmacol. Rev.* **2006**, *58*, 488−520.
(66) Alanazi, A. S.; James, E.; Mehellou, Y. The ProTide Prodrug Technology: Where Next? *ACS Med. Chem. Lett.* **2019**, *10*, 2−5.
(67) Görbig, U.; Balzarini, J.; Meier, C. New CycloAmb-Nucleoside Phosphonate Prodrugs. *Nucleosides, Nucleotides Nucleic Acids* **2007**, *26*, 831−834.
(68) Maintz, D.; Heindel, W.; Kugel, H.; Jaeger, R.; Lackner, K. J. Phosphorus-31 MR Spectroscopy of Normal Adult Human Brain and Brain Tumours. *NMR Biomed.* **2002**, *15*, 18−27.
(69) Gerweck, L. E.; Seetharaman, K. Cellular PH Gradient in Tumor versus Normal Tissue: Potential Exploitation for the Treatment of Cancer. *Cancer Res.* **1996**, *56*, 1194−1198.

(70) Newlands, E.; Stevens, M.; Wedge, S. R.; Wheelhouse, R. T.; Brock, C. Temozolomide: A Review of Its Discovery, Chemical Properties, Pre-Clinical Development and Clinical Trials. *Cancer Treat. Rev.* **1997**, *23*, 35−61.
(71) Muller, F.; Aquilanti, E.; DePinho, R. In Vitro Enzymatic Activity Assay for ENOLASE in Mammalian Cells in Culture. *Protoc. Exch.* **2012**, DOI: 10.1038/protex.2012.040.
(72) Gillies, R. J.; Didier, N.; Denton, M. Determination of Cell Number in Monolayer Cultures. *Anal. Biochem.* **1986**, *159*, 109−113.
(73) Kueng, W.; Silber, E.; Eppenberger, U. Quantification of Cells Cultured on 96-Well Plates. *Anal. Biochem.* **1989**, *182*, 16−19.

https://doi.org/10.1021/acs.jmedchem.2c01039
J. Med. Chem. 2022, 65, 13813−13832